AEDC-TR-70-108

cy.2

INFRARED REFLECTANCE OF CO_2 CRYODEPOSITS

B. E. Wood, A. M. Smith, B. A. Seiber, et al.

ARO, Inc.

July 1970

AEROSPACE ENVIRONMENTAL FACILITY
ARNOLD ENGINEERING DEVELOPMENT CENTER
AIR FORCE SYSTEMS COMMAND
ARNOLD AIR FORCE STATION, TENNESSEE

NOTICES

When U. S. Government drawings specifications, or other data are used for any purpose other than a definitely related Government procurement operation, the Government thereby incurs no responsibility nor any obligation whatsoever, and the fact that the Government may have formulated, furnished, or in any way supplied the said drawings, specifications, or other data, is not to be regarded by implication or otherwise, or in any manner licensing the holder or any other person or corporation, or conveying any rights or permission to manufacture, use, or sell any patented invention that may in any way be related thereto.

Qualified users may obtain copies of this report from the Defense Documentation Center.

References to named commercial products in this report are not to be considered in any sense as an endorsement of the product by the United States Air Force or the Government.

INFRARED REFLECTANCE OF CO_2 CRYODEPOSITS

B. E. Wood, A. M. Smith, B.A. Seiber, et al.
ARO, Inc.

FOREWORD

The research reported herein was sponsored by Headquarters, Arnold Engineering Development Center (AEDC), Air Force Systems Command (AFSC), Arnold Air Force Station, Tennessee, under Program Element 64719F.

The results of the research were obtained by ARO, Inc. (a subsidiary of Sverdrup & Parcel and Associates, Inc.), contract operator of AEDC, AFSC, under Contract F40600-71-C-0002. The work was performed under ARO Projects SW5906 and SW5007 during the period from July 1968 through September 1969. The manuscript was submitted for publication on March 18, 1970.

J. A. Roux was also an author of this report.

This technical report has been reviewed and is approved.

Michael G. Buja
1st Lt, USAF
Research Division
Directorate of Plans
and Technology

Harry L. Maynard
Colonel, USAF
Director of Plans
and Technology

ABSTRACT

In-situ reflectance measurements have been made for carbon dioxide (CO_2) frosts formed on liquid-nitrogen-cooled substrates. The data were obtained spectrally in the wavelength range from 0.5 to 12.0 microns using an infrared integrating sphere. These measurements were made using the hemispherical-angular technique and resulted in the determination of the absolute reflectance. The properties of the CO_2 frosts were studied by forming them on black epoxy paint and polished stainless steel substrates. The CO_2 frosts were found to exhibit an anomalous dispersion reflectance peak at 4.3 microns which was shown to be a very sensitive indication of the presence of solid CO_2. In addition, it was found that CO_2 scatters short wavelength radiation ($\lambda < 1.0$ microns) significantly and is semitransparent for much of the wavelength range between 2.0 and 12.0 microns. The application of these results to other problems associated with cryogenically cooled surfaces is discussed.

CONTENTS

APPENDIX
Illustrations

NOMENCLATURE

a_i	Quadrature weight
$e_{i,\lambda}$	Hemispherically incident energy, w • cm^{-2}
I	Monochromatic intensity, w • cm^{-2} • sr^{-1} • $micron^{-1}$
I_i	Incident intensity, w • cm^{-2} • sr^{-1}
I_r	Reflected intensity, w • cm^{-2} • sr^{-1}
k	Monochromatic absorption coefficient, cm^{-1}
w	$\sigma/(\sigma + k)$
Δw_r	Solid angle of reflection, sr
x	Quadrature point
θ	View angle, deg
λ	Wavelength, microns
μ	Cos ϕ
ρ_{ah}	Angular-hemispherical reflectance
ρ_{ha}	Hemispherical-angular reflectance
σ	Monochromatic scattering coefficient, cm^{-1}
τ	Deposit thickness, mm
$\dot{\tau}$	Deposition rate, microns/sec
$\bar{\tau}$	Local monochromatic optical thickness
ϕ	Angle inside deposit, deg
ψ	Angle of incidence, deg

SECTION I
INTRODUCTION

The thermal radiative properties of cryogenically cooled surfaces are being studied with increased interest as more and more applications of cryogenic coolants appear. The demand for information in this area has greatly exceeded the available supply. Examples of situations where knowledge of the thermal radiative properties of cryogenically cooled surfaces is important are: (1) simulation of cold outer space in ground test facilities by liquid-nitrogen (LN_2)-cooled black surroundings, (2) reflective and emissive properties of cooled optics, (3) formation of frosts on cold surfaces to approximate the formation of planetary frosts (i.e., polar caps on Mars), (4) variation in transmission of cryogenically cooled optical windows caused by thin-film interference effects of thin deposited films, (5) problems associated with absolute calibration of low temperature blackbodies as reference sources, (6) reduction in visibility through spacecraft windows caused by condensation of water and other contaminants.

Many of the previous cryogenic reflective property measurements have suffered somewhat because of the deposits being formed and measured at atmospheric pressure or because the measurements were obtained by a calorimetric technique or within a narrow wavelength range. The present study deals with the reflective properties of LN_2-cooled surfaces in vacuum, with and without the presence of carbon dioxide (CO_2) cryodeposits. The reflectance measurements were made in situ and covered the wavelength range from 0.5 to 12.0 microns.

Absolute reflectance measurements of scattering-type (nonspecular) surfaces are ordinarily made using an integrating sphere. Integrating spheres having magnesium oxide (MgO) or barium sulfate ($BaSO_4$) coatings are limited to wavelengths less than about 2.6 microns because of the low reflectance of the coating for longer wavelengths. However, it was established in Ref. 1 that the usable wavelength range can be extended if powdered sodium chloride (NaCl) is substituted as the sphere coating. By using the NaCl coating, and developing a new radiation source, the usable wavelength range was extended out to 12.0 microns. Cryodeposit reflectance measurements were obtained as functions of wavelength, deposit thickness, substrate material, view angle, and deposition rate of the cryodeposit.

SECTION II
APPARATUS

The infrared integrating sphere (Figs. 1 and 2, Appendix) was composed of two stainless steel hemispheres 8 in. in diameter. The interior of the sphere was coated with powdered reagent-grade NaCl which was applied by first coating the sphere interior with a thin layer of low vapor pressure vacuum grease (10^{-11} torr at 300°K) which served as a bonding agent and then pressing the previously ground NaCl onto the sphere wall until a thickness of approximately 5 mm had been obtained. This technique of coating has the advantage of eliminating highly absorbing water which was present when the water slurry method described in Ref. 1 was used.

The cryosurface (Fig. 3a) was a hollow, 1- by 1-1/2- by 1/2-in., rectangular, stainless steel block which was cooled by continuously flowing LN_2 through it. The test surface was one of the 1- by 1-1/2-in. faces and was either polished stainless steel or was the same face coated with a black epoxy paint. A copper-constantan thermocouple was silver soldered to the surface to allow monitoring of the test surface temperature. In order to restrict the cryopumping area to that of only the cryosurface, the LN_2 supply lines inside the chamber were vacuum jacketed. The entire test surface assembly and LN_2 lines could be rotated without disturbing the vacuum, thereby allowing reflectance measurements to be made as a function of view angle from 0 to 60 deg, measured from the test surface normal.

The pumping system consisted of an ion pump and an LN_2-trapped 4-in. oil diffusion pump backed by a mechanical pump. This system allowed pressures in the 10^{-7} torr range to be routinely achieved. Chamber pressures were monitored using a thermocouple gage and an ion gage.

One of the problems associated with using an infrared integrating sphere is that of obtaining an infrared source which emits enough energy at the longer wavelengths to allow a sufficiently high signal-to-noise ratio in the detection system. In this study, a 1000-w tungsten-halogen lamp was enclosed in a housing which was cooled at both ends (Fig. 3b). This allowed the middle of the housing to heat up to glowing red thereby providing an extra source of infrared energy. The quartz envelope of the lamp does not transmit any appreciable amount of infrared energy beyond 4.0 microns. However, the quartz is a good emitter and the elevated envelope temperature caused by the housing also increases the envelope radiance. Indications are that the elevated temperatures of both housing and envelope contribute to the increase of infrared energy emitted. With this arrangement the source is usable over the wavelength range from 0.3 to at least 25 microns.

Radiation from the source was chopped at 13 Hz and focused onto the wall of the integrating sphere after passing through an NaCl window (Fig. 2). After striking the sphere wall behind the test surface face, the radiation was reflected diffusely throughout the sphere so that the portions of the sphere which were not illuminated directly were uniformly irradiated. Radiation reflected from either the test surface or a portion of the wall not directly irradiated was collected by an off-axis paraboloidal mirror after passing through another NaCl window and focused on the entrance slit of the monochromator.

The monochromator was a prism-type, single-pass system. For most of the measurements an NaCl prism was employed since it was usable over the entire wavelength range from 0.5 to 12.0 microns. In one set of experiments a calcium fluoride (CaF_2) prism was used since it has a much higher dispersion than NaCl in the 1- to 6-micron range. It is difficult to specify the resolution of the monochromator since the prism dispersion and slit width varied with wavelength. The slit width used varied from 0.3 to 2.0 mm. The monochromator and paraboloidal mirror were mounted on a table which could be rotated about the vertical centerline of the viewport, thus allowing radiation from either the test surface or sphere wall to be collected. The detector was a thermocouple which had a sensitivity of 25 microvolts/microwatt. The output from the detector was amplified, synchronously rectified, and displayed on a strip-chart recorder.

Formation of the CO_2 cryodeposit was accomplished by flowing CO_2 gas into the chamber at a known flow rate and allowing the gas to be cryopumped by the LN_2-cooled cryosurface. The flow system was composed of two calibrated standard molecular leaks with a forepressure of 1 atm. The deposition rate, $\dot{\tau}$, of the gas depended on the standard leak used.

SECTION III
PROCEDURE

Prior to cryodeposit reflectance measurements, the integrating sphere system was evacuated to approximately 5×10^{-7} torr and then reflectance measurements were made on the bare test surface for view angles from 0 to 60 deg as measured from the surface normal. The hemispherical-angular technique was used for obtaining spectral absolute reflectance measurements. In this technique the spectral hemispherical-angular reflectance is determined from the relations (Refs. 1 and 2)

$$\rho_{ha}(\theta, \lambda) = \frac{I_r(\theta, \lambda)}{e_{i,h}(\lambda)/\pi} = \frac{I_r(\theta, \lambda)}{I_i(\lambda)} \tag{1}$$

where $I_r(\theta,\lambda)$ is the reflected intensity within the small collection solid angle Δw_r (0.02 sr) inclined at the angle θ and $e_{i,h}(\lambda)$ is the hemispherically incident energy with the associated diffusely incident intensity $I_i(\lambda)$. Since the same collection solid angle, Δw_r, is used for both quantities, the absolute reflectance can be obtained from Eq. (1). Even though the exact quantities $I_r(\theta,\lambda)$ and $I_i(\lambda)$ are not measured, the detector outputs are directly related to these quantities by multiplicative constants which depend on the transfer optics and detection system. The measurements were accomplished by first viewing the sample and obtaining a detector output for a given wavelength. This was followed by viewing a portion of the sphere wall (not directly irradiated) at the same wavelength and again recording the detector output. Since the sphere wall is uniformly irradiated by multiple reflections, the intensity of the radiation reflected from the sphere wall is equal to the intensity incident on the test surface. From these two detector outputs, the absolute reflectance can be determined from Eq. (1).

This same procedure was carried out for other wavelengths and, by rotating the cryosurface, similar measurements were obtained for other view angles. It is shown (Ref. 2) that the hemispherical-angular reflectance, ρ_{ha}, is equivalent to the angular-hemispherical reflectance, ρ_{ah}, provided the same solid angles are used and that the view angle θ for ρ_{ha} is equal to the incidence angle, ψ, for ρ_{ah}. Therefore, the term view angle in this report corresponds to the more commonly used term: angle of incidence.

After obtaining the test surface reflectance as a function of wavelength and incidence angle, LN_2 was used to cool the test surface to 93°K. After valving off the integrating sphere from the pumping system the CO_2 gas flow into the sphere was started with the CO_2 freezing out on the cryosurface. By allowing the gas to condense on only the test surface, a given flow time resulted in a certain thickness, τ, of the deposit. The average thickness over the entire surface could be calculated by knowing the mass flow

rate, cryosurface pumping area, and density of deposit. The cryosurface pumping area was 40.2 cm^2, and the mass flow rate either 2.25×10^{-3} gm/sec or 2.39×10^{-4} gm/sec. The cryodeposit density was taken to be 1.67 (Ref. 3) since the deposits were formed at pressures approximately the same as those in Ref. 3. In-situ thickness measurements were made in order to verify the deposit thickness as calculated. This was done using thin-film interference techniques discussed in Refs. 3 through 5. This technique requires knowing the refractive index of the deposits, and these values are reported in Ref. 3. The thicknesses determined by the two methods were in good agreement.

The chamber pressure during deposition varied between 10^{-3} and 10^{-1} torr and depended on the flow rate and cryodeposit thickness. For the majority of the measurements the deposition pressure varied between 10^{-2} and 10^{-1} torr. After each thickness of deposit had been formed, reflectance measurements were made over the complete wavelength range from 0.5 to 12.0 microns. This procedure was continued until the deposit had reached the desired thickness (usually 3 to 4 mm). At the conclusion of the reflectance measurements for the thickest deposit, the chamber was brought up to atmospheric pressure with dry N_2. The test surface was withdrawn and immediately the deposit thickness was checked by means of a calibrated probe. Although relatively crude, this served to establish the validity of the thickness measurement and to ensure that nonuniform pumping was not a problem. In all cases the thicknesses measured by this technique were in agreement with thicknesses determined from the mass flow calculation method discussed previously.

SECTION IV
RESULTS

4.1 BLACK EPOXY PAINT SUBSTRATE

The reflectances of CO_2 cryodeposits formed on an LN_2-cooled black epoxy paint substrate are shown in Fig. 4 for wavelengths between 0.5 and 12.0 microns. The view angle, θ, was 10 deg for all thicknesses. These deposits were formed using a deposition rate of 0.335 microns/sec which resulted in a deposition pressure from 1×10^{-2} to 5×10^{-2} torr, for deposits 1.7 mm thick or less. For the 3.4-mm-thick deposit the final pressure during deposition was 1.25×10^{-1} torr. The flow time required to form a deposit 3.4 mm thick was approximately 2-3/4 hr.

Figure 4a shows the reflectance of the bare substrate before deposition. It can be seen that the reflectance is essentially independent of wavelength with only a slight increase from 5 percent up to 8 or 9 percent in the vicinity of 9 to 11 microns. Figures 4b to f show the reflectance of the various thicknesses of cryodeposit ranging from 0.13 mm up to 3.38 mm. As can be seen by comparison of the data for different thicknesses, the reflectance begins to increase first at the short wavelengths ($\lambda < 1.5$ microns) and continues to increase for the long wavelengths as the deposit thickness is increased. The increased reflectance at the shorter wavelengths has been previously reported (Ref. 5). For wavelengths greater than about 2.0 microns the reflectance is shown to be less than the bare substrate reflectance for the 0.13- and 0.23-mm-thick deposits. This is also typical of the reflectance for shorter wavelengths ($\lambda < 2.0$ microns) but the effect shows

up for deposits thinner than any shown in Fig. 4. As the thickness is increased further, the reflectance increases for all wavelengths as can be seen from Figs. 4b to f. For the thickest deposit investigated, τ = 3.38 mm, the reflectance rose to about 77 percent for λ = 0.5 microns but dropped off rapidly with increasing wavelength.

In Figs. 4b and c the single most prominent spectral feature is the sharp rise in reflectance in the region of 4.3 microns. As the thickness of the deposit increases this feature becomes less prominent because of the increase in bulk scattering of other wavelengths around the 4.3-micron region. The reflectance peak is attributed to anomalous dispersion (Ref. 6) wherein a strong absorption band in a liquid or solid has associated with it a very high index of refraction so that both absorption and reflection coefficients are quite high. It is well known that in the gaseous phase, CO_2 exhibits its strongest absorption at 4.25 microns. As can be seen in Figs. 4b through f the rapid increase in reflectance in this region results in a powerful technique for identifying the pressure of solid CO_2. The peak at 4.3 microns has been seen for deposits as thin as 1 micron.

For CO_2 deposits equal to or less than 1.70 mm thickness there is relatively little spectral structure seen in the reflectance spectra in Fig. 4 because of the transmission of the deposit and the highly absorbing black substrate. However, for the 3.38-mm-thick deposit (Fig. 4f) the scattering increased significantly which enhances the absorption bands because of the increased reflectance for the nearby wavelengths. Absorption bands can now be seen to occur at 2.0 microns, 2.85 microns, and what appears to be bands at 3.85 and 4.55 microns. However, the latter two are really part of the strong absorption band centered around 4.25 microns with the reflectance peak occurring essentially in the middle of the absorption band. Other spectral features to be seen in Fig. 4f are a broad reflectance increase extending from 7.9 to 10.5 microns and a gradual rise in reflectance from 10.5 to 12.0 microns. For all of the CO_2 deposits formed on the black substrate, it can be seen that the reflectance will be less than 20 percent for wavelengths between 2.7 and 12.0 microns. This could be a result of the deposits being low reflectors (high absorbers) or the deposits being somewhat transparent with most of the energy being absorbed by the black substrate. As shown later, the latter is the most significant factor.

The reflectance dependence on deposit thickness is presented in Fig. 5. The view angle is again 10 deg and the dependence on thickness is shown for the selected wavelengths of 0.5, 1.0, 2.0, 4.0, 8.0, and 12.0 microns. For 0.5-micron radiation, the 3.38-mm-thick deposit effectively behaves as one of infinite thickness since the reflectance has leveled off at this thickness. However, for λ = 1.0 and 2.0 microns, the reflectance is still increasing with thickness at 3.38 mm. The λ = 2-micron curve is essentially linear with deposit thickness above τ = 0.4 mm. At the other three wavelengths, the deposit reflectance is still dependent on thickness at 3.38 mm but much less so than for the 2.0-micron curve. The increase in reflectance for λ = 8.0 and 12.0 microns is only slight because of the relatively small scattering coefficient at these wavelengths. For the λ = 4.0-micron curve, very little thickness dependence is present, as expected, since the CO_2 deposit is highly absorbing at this wavelength.

As mentioned earlier the view angle, θ, was 10 deg. The dependence on this parameter for the same deposits discussed earlier is shown in Figs. 6a through d for view

angles from 0 (normal to the surface) up to 60 deg and for wavelengths of 0.5, 1.0, 2.0, and 8.0 microns. For the bare black substrate the reflectance at 60 deg is about 6 or 7 percent greater than for a view angle of 60 deg (e.g., for 0.5-micron radiation the reflectance for 0-deg view angle is approximately 5 percent and for 60 deg is about 11 percent). For the thicker deposits the reflectance was found to increase by 10 to 13 percent as the view angle increased from 0 to 60 deg. It can be seen that the angular dependence is present for all deposit thicknesses and for all four wavelengths.

To determine the reflective properties of thin CO_2 deposits on the black epoxy paint and to determine possible deposition flow rate effects, a series of measurements was made using a deposition rate, $\dot{\tau}$, of 0.0355 microns/sec which is about a factor of 10 less than the deposition rate used for the previously discussed measurements. For these investigations, the wavelength range covered was from 0.5 to 5.0 microns since it had already been established that relatively little change was observed for the longer wavelength radiation for the thinner deposits. In Fig. 7, the reflectances of thin CO_2 deposits formed at a deposition rate of 0.0355 microns/sec on the black substrate are shown for deposits 2, 27, 54, 108, and 215 microns thick. Notice that even for the thinnest deposit, 2 microns thick, the 4.3-micron anomalous dispersion band is already quite apparent. The only significant change in reflectance for all thicknesses and wavelengths, other than that for λ at 4.3 microns, is the gradual increase in reflectance for wavelengths between 0.5 and 1.5 microns attributable to internal scattering. In the thickness region of overlap between Figs. 4 and 7, it appears that the deposits formed at the lower deposition rate are less reflecting. For example, at 231 microns, for the larger deposition rate, the reflectance is about 32 percent at λ = 0.5 microns, whereas for 215 microns formed at the lower deposition rate, the reflectance is only 21 percent at the same wavelength. For the 2-micron-thick deposit, the reflectance is substantially lower than the bare substrate reflectance for wavelengths less than 1 micron. This effect is usually present for all wavelengths although it is not so noticeable in Fig. 7. The deposition pressure for the lower deposition rate varied from 10^{-3} torr for the 2-micron-thick deposit up to 2×10^{-2} torr for the 215-micron-thick deposit and was a little lower than for the deposits formed at the higher deposition rate.

4.2 STAINLESS STEEL SUBSTRATE

To understand more fully the radiative properties of CO_2 deposits, a polished LN_2-cooled stainless steel substrate was employed. This was the same test surface used in the previous measurements but with the black paint removed and the surface repolished. In Fig. 8a the reflectance of the bare polished stainless steel surface is shown with an absorption band occurring around 3.0 microns. This band could not be eliminated although various methods were attempted such as mild bakeout under vacuum, repolishing with various types of abrasives, and finally, cleaning with Freon® in an ultrasonic cleaner. Since the band shows up at 3.0 microns and increased scatter in the reflectance data is seen in the 5- to 6-micron region, it would appear that some form of water was permanently entrenched in the steel. As shown in Figs. 8b through g reflectances of CO_2 deposits of thicknesses 0.13, 0.23, 0.44, 0.86, 1.70, and 3.38 mm were formed on the stainless steel substrate. The pressure during deposition varied from 2×10^{-2} to 4×10^{-2} torr for the 0.13- to 0.86-mm-thick deposits, was 10^{-1} torr for the 1.7-mm-thick deposit, and was 2×10^{-1} torr for the 3.38-mm-thick deposit. Notice that

for the 0.13-mm-thick deposit the reflectance at the shorter wavelengths (λ = 0.5 microns) decreased to 40 percent from the bare substrate reflectance of 58 percent. Further increase in deposit thickness, however, caused the reflectance to increase because of internal scattering until eventually it leveled off. For longer wavelengths, $\lambda > 2.0$ microns, the reflectance is influenced by strong absorption bands in some regions, and a gradual decrease in the reflectance is noted in other wavelength regions as the thickness is increased. It was expected in these highly reflecting regions that the reflectance would gradually decrease with thickness since only a slight increase in reflectance was seen for similar thicknesses of deposits formed on the black surface. This indicates that the scattering coefficient and absorption coefficient are relatively small and that the deposit is semitransparent in these wavelength regions. In contrast to the reflectance curves for the black epoxy paint substrate, the absorption bands are quite pronounced even for the smaller deposit thicknesses. In the wavelength regions near these bands the deposits are somewhat transparent with the result that the stainless steel substrate reflectance continues to influence the amount of radiation reflected. The high reflectance at wavelengths near the absorption bands accentuates the absorption in these regions.

By comparing the reflectance data for deposits of equal thickness formed on the two substrates, it becomes apparent that the CO_2 deposits transmit appreciably in the wavelength region from 1 to 12 microns. If the deposits were not somewhat transparent, the reflectances observed for cryodeposits of equal thickness formed on the two different substrates would be more nearly the same. For instance, the reflectance at 5.5 microns for a 3.38-mm-thick deposit on stainless steel is 65 percent, whereas for an equal thickness on the black substrate the reflectance is only 19 percent. This indicates that even at this relatively large thickness the substrate reflectance still influences the determination of the cryodeposit-substrate complex reflectance which can only be explained by the deposit being transparent for radiation at these wavelengths.

As mentioned previously, the absorption bands of CO_2 show up more clearly in Fig. 8 than in Fig. 4. Absorption bands for the 3.38-mm-thick deposit can be seen to be centered around 2.0, 2.85 to 3.0, 4.3, 6.1, 6.85, and 7.55 microns. The location of the absorption band in the 2.85- to 3.0-micron region seemed to vary with deposits. For instance in Fig. 8b the band is centered at 2.85, but thicker deposits exhibited the same absorption band centered at 3.0 microns. This variation was also seen for other deposits (not shown). As shown in Fig. 8, the reflectance peak at 4.3 microns is again present but is not so noticeable as in Fig. 4. Notice, however, that the peak heights are about the same in each case (20 to 25 percent). For 10.5 microns, there is a significant reduction in reflectance. For the 3.38-mm-thick deposit the reflectance dropped to 20 percent at 12.0 microns.

The change in reflectance as the deposit thickness is varied is shown in Fig. 9a for wavelengths of 1.0, 4.0, and 8.0 microns. These data are taken from Fig. 8 so only reflectance data at given thicknesses are shown. Although the 1.0-micron curve shows an initial decrease to 42.5 percent, this is approximate since the decrease may have been greater for a slightly smaller or larger thickness. Further increase in deposit thickness causes the reflectance to rise above the initial bare surface reflectance as discussed earlier. The 4.0-micron curve shows the considerable absorption characterized by the continually

decreasing reflectance curve with thickness. In contrast, the 8.0-micron curve decreases slowly until reaching a minimum for deposits approximately 1 mm thick and is then followed by a slight rise. This further indicates that CO_2 is only weakly absorbing at this wavelength. Figure 9b shows a curve similar to those in Fig. 9a but this time the reflectance was monitored continuously at a given wavelength, $\lambda = 0.7$ microns, as the deposit was being formed. This curve shape was more characteristic of reflectance versus thickness curves on stainless steel than was the 1.0-micron curve shown in Fig. 9a. The curve for $\lambda = 0.7$ microns in Fig. 9b does not rise quite as rapidly with thickness. This could have been caused by a slight variation in the structure of the two deposits even though they were formed under essentially the same conditions, such as deposition rate, pressure, and cryosurface temperature. The behavior of the reflectance versus thickness curve in Fig. 9b is interesting in that it has a sharp decrease initially, followed by a more gradual decrease until reaching a minimum, and then increasing until the reflectance levels off at a value much higher than the initial reflectance. The reason for this behavior will be explained in detail later in Section 4.3.

The reflectance dependence on view angle for a 0.84-mm-thick CO_2 deposit on stainless steel is presented in Fig. 10. The dependence on angle is greater for $\lambda = 0.5$ and 1.0 microns than for the other wavelengths presented. Generally speaking, however, there was relatively little variation with view angle for any of the deposits formed on the stainless steel substrate. This is in contrast with the results obtained using the black substrate which showed a significant dependence on view angle for nearly all wavelengths and deposit thicknesses.

Figure 11 shows the reflectance (for $0.5 \leqslant \lambda \leqslant 5.1$ microns) of a bare polished stainless steel surface and the surface with CO_2 deposits 3.0, 59, and 218 microns thick formed at the lower deposition rate, 0.0355 microns/sec. The bare surface reflectance was somewhat less than that shown in Fig. 8a because of an optical finish of lesser quality than that shown in Fig. 8a. Notice that the reflectance changes significantly even for these relatively thin deposits. For the 3.0-micron-thick deposit, thin-film interference patterns can be seen along with an overall reduction of about 5 to 10 percent from that for the bare surface. For the 59-micron-thick deposit, the interference patterns are gone but the reflectance has been decreased further. The absorption bands at 2.85 and 4.3 microns also are seen to be already quite strong for the 59.0-micron thickness. For the 218-micron (0.218-mm)-thick deposit, the reflectance is reduced even more. Notice also that for this deposit thickness the reflectance at the shorter wavelengths ($\lambda < 1.0$ microns) is between 35 and 40 percent, which is considerably less than the reflectance of the comparable thickness (0.230 mm) of deposit formed at the higher deposition rate and shown in Fig. 8c.

4.3 ANALYTICAL RESULTS

Figure 9b shows that the reflectance initially undergoes a decrease, then descends to a minimum, and finally the reflectance increases with deposit thickness until reaching a plateau. Because of the occurrence of this interesting and unexpected phenomenon an analytical investigation was conducted to obtain a fundamental understanding of cryodeposit reflectances and their variation with thickness, view angle, substrate, and

refractive index. The theoretical study was conducted with the objective of formulating a mathematical model for the cryodeposit reflectance based on the results of past and present experimental work.

In the search for a realistic reflectance model several combinations of boundary conditions were considered for the substrate and vacuum deposit interface. Based on the magnitude of the reflectances and the general trend of the data gathered in this report and in Ref. 1, it was decided that the best model would be to take the substrate and vacuum deposit interfaces as Fresnel surfaces. The internal structure of the deposit was considered as an absorbing and isotropic scattering medium; that is, the probability of energy being scattered into every direction is equal.

This model for the cryodeposit reflectance required the solution of the radiative transport equation

$$\frac{dI}{d\bar{\tau}} = \frac{-I}{\mu} + \frac{w}{2\mu}\int_{-1}^{1} I(\mu)\, d\mu \tag{2}$$

where

$$\bar{\tau} = \int_{0}^{\tau} (k + \sigma)\, d\tau \tag{3}$$

is the local monochromatic optical thickness at physical thickness τ. This transport equation is an integro-differential equation and was reduced to a system of ordinary linear differential equations by the method of discrete ordinates which employed the Gaussian quadrature:

$$\int_{-1}^{1} f(x)dx = \sum_{j=1}^{m} f(x_j)\, a_j \tag{4}$$

where x_j is the quadrature point and a_j is the quadrature weight. Therefore,

$$\frac{dI(\bar{\tau}, \mu_i)}{d\bar{\tau}} = \frac{I(\bar{\tau}, \mu_i)}{\mu_i} + \frac{w}{2\mu_i}\sum_{j=1}^{m} I(\bar{\tau}, \mu_i)\, a_j \tag{5}$$

where i = 1, 2, 3, ..., n

The solution of the system of simultaneous differential equations together with the diffuse irradiance boundary conditions is extremely lengthy and complex and will be discussed in detail in a future report. It should suffice to mention that the system of equations was solved numerically using the Milne predictor-corrector method.

The theoretical investigation was conducted with the point of view of matching the hemispherical-directional reflectance measured for cryodeposits. This led to a computer program that employs two experimental data points (the hemispherical-directional reflectance at two different thicknesses) to calculate a

monochromatic absorption and scattering coefficient. Once the coefficients were calculated they were used to "predict" reflectance values at other cryodeposit thicknesses.

Figure 12 shows a comparison between the theoretical and experimental results for a CO_2 cryodeposit on a stainless steel substrate at $\lambda = 0.7$ microns. The arrows indicate the two data points used in the computer program to calculate the monochromatic absorption and scattering coefficients. All other points were predicted using these coefficients. The theoretical results are in very good agreement with the data which indicates that the analytical model proposed is realistic.

Since the cryodeposit reflectance model has proved to be a reasonable one, it can be used to explain the shape of the curve in Fig. 9b. For small deposit thicknesses near zero, there is a sharp (almost discontinuous) drop in reflectance attributable to the relative refractive index change. This reflectance decrease is from 0.49 to 0.388 and is denoted as the first decrease. As the deposit thickness increases there is a second reflectance decrease from 0.388 to 0.325. In view of the theoretical model, this second decrease is a result of internal scattering occurring in the deposit. Some of the internally scattered intensity is incident internally on the vacuum-deposit interface at angles greater than the critical angle and therefore undergoes total internal reflection. The reflectance decreases since the thickness increase causes a higher probability that more intensity will be scattered past the critical angle and thus eventually will be absorbed by the substrate before being rescattered. However, as the thickness increases further, the total internally reflected intensity has an even higher probability of being rescattered before reaching the substrate and thus being rescattered into directions less than the critical angle and hence partially escaping the cryodeposit. At larger thicknesses the internal scattering dominates, causing more intensity to escape the deposit because of the rescattering effect and therefore resulting in a reflectance that then monotonically increases with thickness. The deposit is by then so thick that each beam of intensity is multiply scattered and is thus less likely to reach the absorbing substrate. For greater deposit thicknesses, the curve levels off to a reflectance plateau of about 0.71. The reflectance should stay at approximately this value as the thickness increases further since there is a small but finite amount of absorption as indicated by the absorption coefficient shown on the figure.

SECTION V
DISCUSSION

The results presented in Figs. 4 through 11 show the reflectance of CO_2 cryodeposits formed on stainless steel and black epoxy paint substrates and ranging from 2 microns to 3.38 mm in thickness. These thicknesses cover the range of concern for most of the situations listed in the Introduction. From the results discussed previously, it is apparent that several aspects should be considered in determining the reflectance of CO_2 frosts: wavelength, deposit thickness, substrate material, view angle, pressure during formation, and rate of formation.

Possible applications of these data to some of the problems mentioned earlier are apparent. The presence of thin CO_2 deposits ($\tau < 100$ microns) on black surfaces will

have a relatively small effect; the reflectance in the visible and near-infrared wavelength range will show only a slight increase; and for infrared radiation the reflectance will be reduced for these same thicknesses. For even thinner deposits, $\tau < 20$ microns, the reflectance in the visible and near-IR range can also be reduced. For most applications in space simulation chambers these changes will be negligible. The reflectance changes for the larger thicknesses ($\tau > 100$ microns), however, will not be negligible.

The thin deposits may also have a significant effect in the calibration of low temperature blackbody reference sources. The presence of thin deposits will, in general, increase the emittance, expecially in the wavelength range from 3.0 to 12.0 microns. Although no data were taken for $\lambda > 12.0$ microns, it is believed that emittance values would also be increased for longer wavelengths. With the current interest in absolute calibration of low temperature blackbodies, these thin-film effects become increasingly important.

Cooled optics are often used in situations where the surrounding pressure is relatively high, e.g., in balloons or aircraft. Under such conditions it is impossible to keep cryogenically cooled surfaces free from contamination attributable to condensation of CO_2 and H_2O gases. For determination of effects of the CO_2 frosts on cooled optics (such as mirrors), Fig. 11 summarizes some of the problems that would be encountered. For example, the 3.0-micron-thick deposit formed on a polished stainless steel surface causes the reflectance to decrease overall and to vary with wavelength because of the phenomenon of thin-film interference (Refs. 3 to 5). These interference peaks and valleys were seen for deposits up to approximately 10 microns thick. This phenomenon would cause a similar wavelength-dependent increase and decrease in the transmission of cooled windows and lenses. For a thicker deposit, 59.0 microns, the reflectance is reduced by from about 10 to 15 percent over most of the wavelength range from 0.5 to 5.0 microns. In the region of the 2.85- and 4.3-micron absorption bands the reflectance as expected is reduced considerably more. For most applications of cooled optics, deposits thicker than 60 microns on a cooled optical surface will render it unusable. In addition to the reflectance considerations, the increase in emittance, and the reduction in image quality attributable to scattering by the cryodeposit will also have to be considered.

Finally, the recent findings of the Mariner 6 and Mariner 7 probes have increased the interest in the reflective properties of both carbon dioxide and water frosts. According to Herr and Pimentel (Ref. 7) the reflectance data obtained from Mariners 6 and 7 indicate that the Martian polar caps are carbon dioxide. They also reported that absorption bands at 3.34 and 3.04 microns, which had earlier been designated as methane and ammonia bands, respectively, were also caused by CO_2. They verified this by obtaining the same absorption bands for CO_2 frosts formed under laboratory conditions. This was the first reported observation of these two bands for CO_2. These two bands were not seen in the measurements presented in Figs. 4, 7, 8, and 12, and the data in Figs. 8 and 11 were, like the laboratory data of Herr and Pimentel, for CO_2 formed on stainless steel.

In order to obtain higher-resolution data, the NaCl prism was replaced by a CaF_2 prism. Figure 13 shows the results of the reflectance of a CO_2 deposit 4 mm thick. The

pressure during deposition was 1.80×10^{-1} torr or less and the view angle, θ, was 18 deg. With the higher resolution an absorption band was seen at approximately 3.36 microns which is probably the same band reported by Herr and Pimentel in Ref. 7. The other band reported by Herr and Pimentel at approximately 3.04 microns was not seen. The anomalous dispersion reflectance peak at 4.3 microns was not observed in the reflectance data of the Martian polar cap shown by Herr and Pimentel in Ref. 7. This was probably because the reflected radiation from the polar cap was in turn absorbed by the surrounding CO_2 gas. However, in a later article (Ref. 8) Herr and Pimentel report seeing the anomalous dispersion peak at 4.3 microns but not while viewing the polar caps but when viewing the bright limb of the planet. This indicated to them that the solid CO_2 was somehow suspended above the planet in some type of particle cloud in a manner not completely understood. This observation establishes conclusively the presence of solid CO_2 either on the surface or in the atmosphere of Mars. Herr and Pimentel suggest that since the peak does show up, the CO_2 cloud must be suspended high enough up so that the atmosphere can be considered optically thin as far as gaseous absorption in the 4.3-micron region is concerned.

In Ref. 8 the anomalous dispersion peak at 4.3 microns in the laboratory data is much sharper and higher in magnitude than the peaks shown in the Mariner data. The magnitude and sharpness of the peak in addition to instrument resolution may depend on the pressure and method by which the deposit was formed. In the measurements presented here, the reflectance of the peaks was, in general, 15 to 25 percent. Although no scale labels were shown in Ref. 8, it is obvious that the peaks observed in their laboratory data are of greater relative magnitude than those in this study or in the Mariner data. No indication was given of the pressure level during deposition of the deposits used in Ref. 8. However, Keegan and Weidner (Ref. 9) measured the reflectance of CO_2 frosts formed at atmospheric pressure, and they too observed a sharp peak at 4.3 microns with reflectance peaks of 40 to 45 percent. They also made similar measurements on crushed dry ice and observed reflectance peaks of only about 25 percent. In one experiment in the present study (data not shown) the deposit was formed at relatively high pressure, $P > 1$ torr. In this instance the 4.3-micron peak reached a value of 50 percent. It would seem from the scattered bits of data that the CO_2 frosts formed at higher pressures exhibit higher reflectance values at 4.3 microns. If this speculation about the influence of pressure is correct, the assumption of formation of the CO_2 particle cloud in the upper atmosphere of Mars is strengthened since the relatively small magnitude of the peak would correspond to formation at lower pressures. This would be consistent with Herr and Pimentel's assumption that the location of the CO_2 clouds would be above the Martian surface where the atmosphere could be considered optically thin. The reduction in prominence of the band may also be attributable to the particle cloud suspended in the atmosphere at a level where the CO_2 gas density is not optically thin but dense enough to partially attenuate the 4.3-micron peak with the result that the peak is only decreased considerably rather than being eliminated entirely.

Further comparison of the data of Herr and Pimentel of Ref. 7 with Fig. 13 indicates some significant differences. First, Herr and Pimentel show a strong broad absorption band in the vicinity of 5.3 microns, which is even stronger than the 4.3-micron CO_2 band. This was not observed in any of the measurements reported

herein, nor was this band seen in Ref. 9, where CO_2 frosts formed at atmospheric pressure were studied. This might be caused by the difference in the ordinate scale since this report and Ref. 9 measured the reflectance, whereas Herr and Pimentel in Refs. 7 and 8 use intensity which probably corresponds to detector output. The present study and Ref. 9 both observed narrow absorption bands near 5.0 and 5.24 microns, whereas neither of these two bands were reported by Herr and Pimentel in Ref. 7 either in the Martian polar cap data or in their laboratory data. Bands located near these two were seen in the CO_2 gas in the Martian atmosphere and were found to be at 4.76 and 5.13 microns.

As shown in Fig. 13, there is a broad absorption band centered around 3.0 microns which is probably attributable to a small trace of water which was present in the chamber from outgassing. The band centered around 6.2 microns also indicates the presence of water impurities even though the chamber was initially pumped down to approximately 5×10^{-7} torr. To determine the effect of water contamination in this wavelength range, a thin film of water frost (τ = 11 microns) was formed on top of the 4-mm-thick CO_2 deposit. Figure 14 shows the results. Even for this small thickness, the reflectance was reduced for all wavelengths with the most noticeable reductions occurring in the 2.9- to 3.4-micron region and the 5.0- to 6.4-micron range. This means that the 3.04-micron band seen in Ref. 7 would not have been seen in Fig. 13 because of the trace of water which obscured any recognizable band in this wavelength region. However, it is possible that the slight band at 3.04 microns of Ref. 7 may also be attributable to water particles sparsely scattered throughout the polar cap.

SECTION VI
SUMMARY

In-situ reflectance measurements on LN_2-cooled surfaces within a vacuum were carried out in a powdered NaCl-coated integrating sphere. The wavelength range investigated was from 0.5 to 12.0 microns which considerably extended the operating wavelength range over that for conventional integrating spheres (0.3 to 2.5 microns).

Reflectance measurements of CO_2 cryodeposits formed on surfaces coated with black epoxy paint and on bare stainless steel surfaces were obtained for deposit thicknesses ranging from 2 microns to 4.0 mm. A reflectance peak at 4.3 microns was found to be attributable to anomalous dispersion. The presence of this peak in the reflection spectra was shown to be a very sensitive method of detecting solid CO_2 since a deposit only 2 microns thick on black epoxy paint shows the peak quite clearly.

The CO_2 deposits absorbed strongly at 2.0, 2.85, and in the vicinity of 4.3 microns. With a higher resolution instrument, weaker absorption bands were also seen at 3.36, 5.0 and 5.24 microns. Thick CO_2 deposits were highly reflecting at the shorter wavelengths ($\lambda < 2.0$ microns) and transmitted appreciably at longer wavelengths (excluding absorption bands). The reflectance was found to be dependent on view angle for all wavelengths for CO_2 formed on the black epoxy paint. Less dependence on view angle was seen for the deposits formed on the stainless steel substrate.

Finally, the applicability of the experimental results to several current problems was discussed. These current problems included determination of the composition of the Martian polar caps, thermal radiative properties of cooled optics, effects on space simulation chamber cold walls, effects on emittance of low temperature blackbody reference sources, and problems associated with thin-film interference reflection and transmission phenomena of optical surfaces.

REFERENCES

1. McCullough, B. A., Wood, B. E., Smith, A. M., and Birkebak, R. C. "A Vacuum Integrating Sphere for In Situ Reflectance Measurements at 77°K from 0.5 to 10.0μ." Progress in Astronautics and Aeronautics, Vol. 20, Academic Press, Inc., New York, 1967, p. 137.

2. Sparrow, E. M. and Cess, R. D. Radiation Heat Transfer. Brooks/Cole Publishing Company, Belmont, California, 1966, p. 57.

3. Müller, P. R., Frost, W. and Smith, A. M. "Measurements of Refractive Index, Density, and Reflected Light Distributions for Carbon Dioxide and Water Cryodeposits." AEDC-TR-69-179 (AD692714), September 1969.

4. Smith, A. M., Tempelmeyer, K. E., Müller, P. R. and Wood, B. E. "Angular Distribution of Visible and Near IR Radiation Reflected from CO_2 Cryodeposits." AIAA Journal, Vol. 7, No. 12, 1969, p. 2274.

5. Wood, B. E. and Smith, A. M. "Spectral Reflectance of Water and Carbon Dioxide Cryodeposits from 0.36 to 1.15μ." AIAA Journal, Vol. 6, No. 7, 1968, p. 1362.

6. Jenkins, F. A. and White, H. E. Fundamentals of Optics, McGraw-Hill Book Co., Inc., 1957, p. 469.

7. Herr, K. C. and Pimentel, G. C. "Infrared Absorptions near Three Microns Recorded over the Polar Cap of Mars." Science, Vol. 166, No. 3904, 1969, p. 498.

8. Herr, K. C. and Pimentel, G. C. "Evidence for Solid Carbon Dioxide in the Upper Atmosphere of Mars." Science, Vol. 167, No. 3914, 1970, p. 47.

9. Keegan, H. J. and Weidner, V. R. "Infrared Spectral Reflectance of Frost." Journal of the Optical Society of America, Vol. 56, No. 4, 1966, p. 523.

APPENDIX
ILLUSTRATIONS

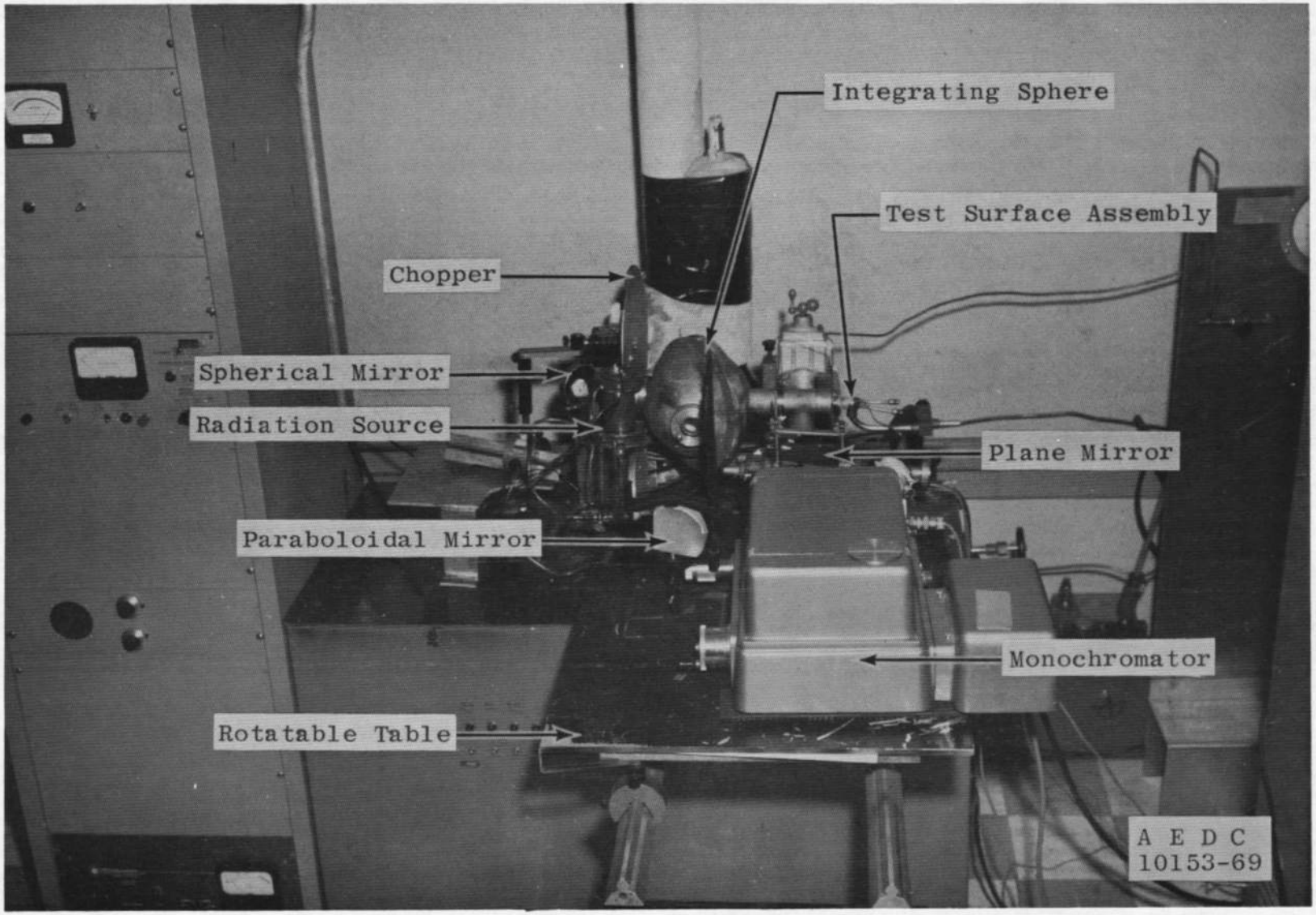

Fig. 1 Infrared Integrating Sphere and Optical Systems

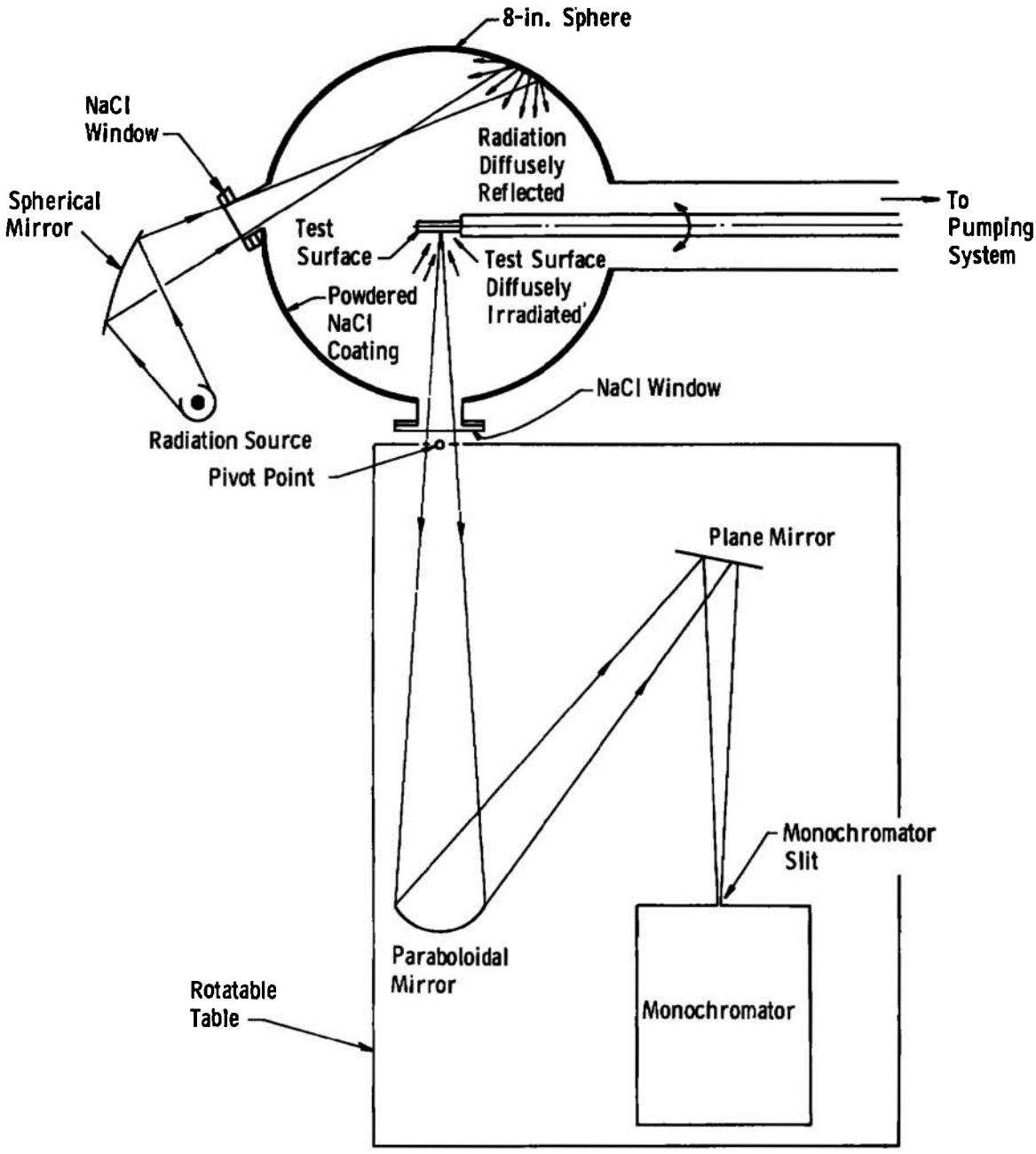

Fig. 2 Schematic of Infrared Integrating Sphere and Components

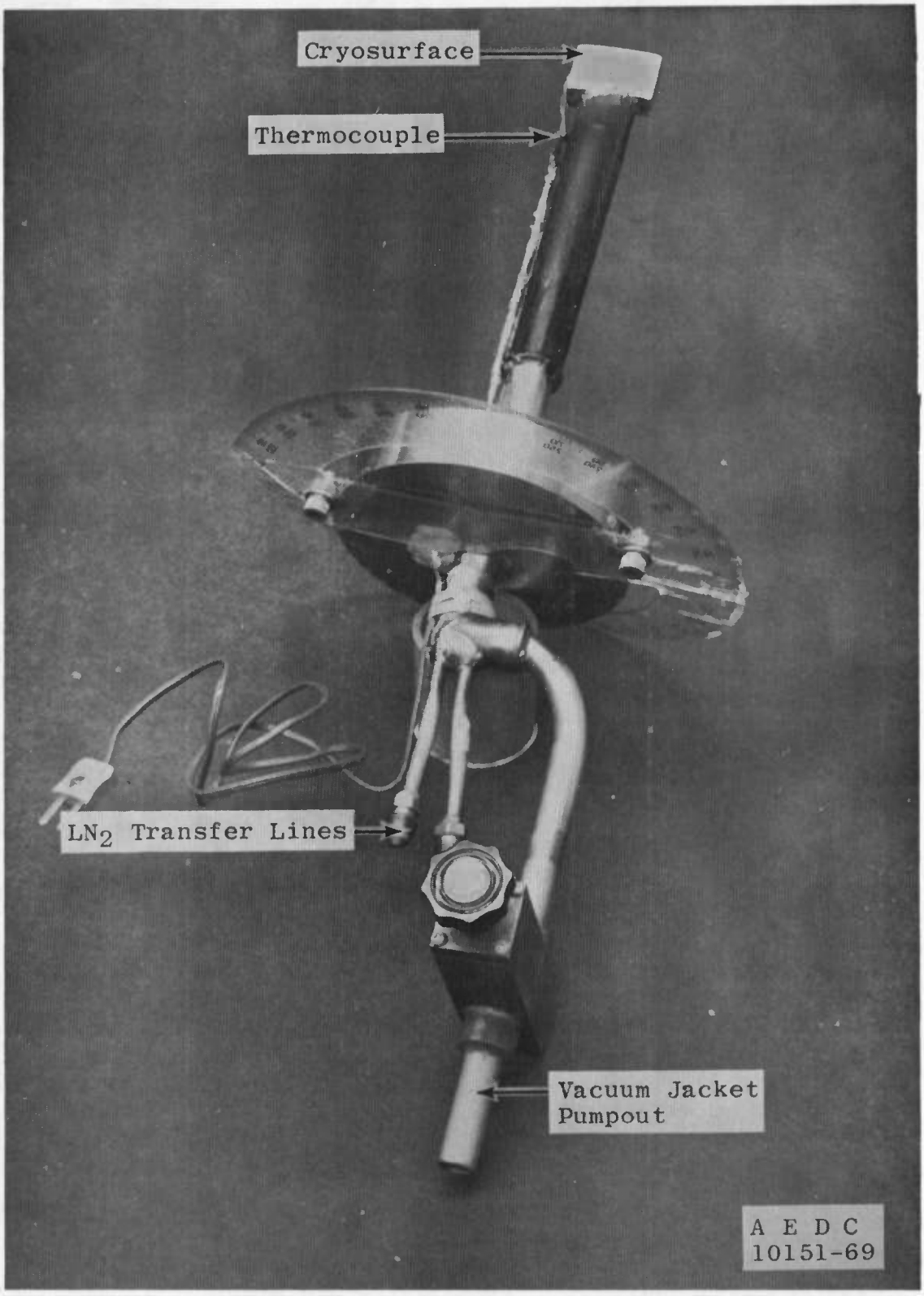

a. Cryogenic Test Surface Assembly

Fig. 3 Test Apparatus

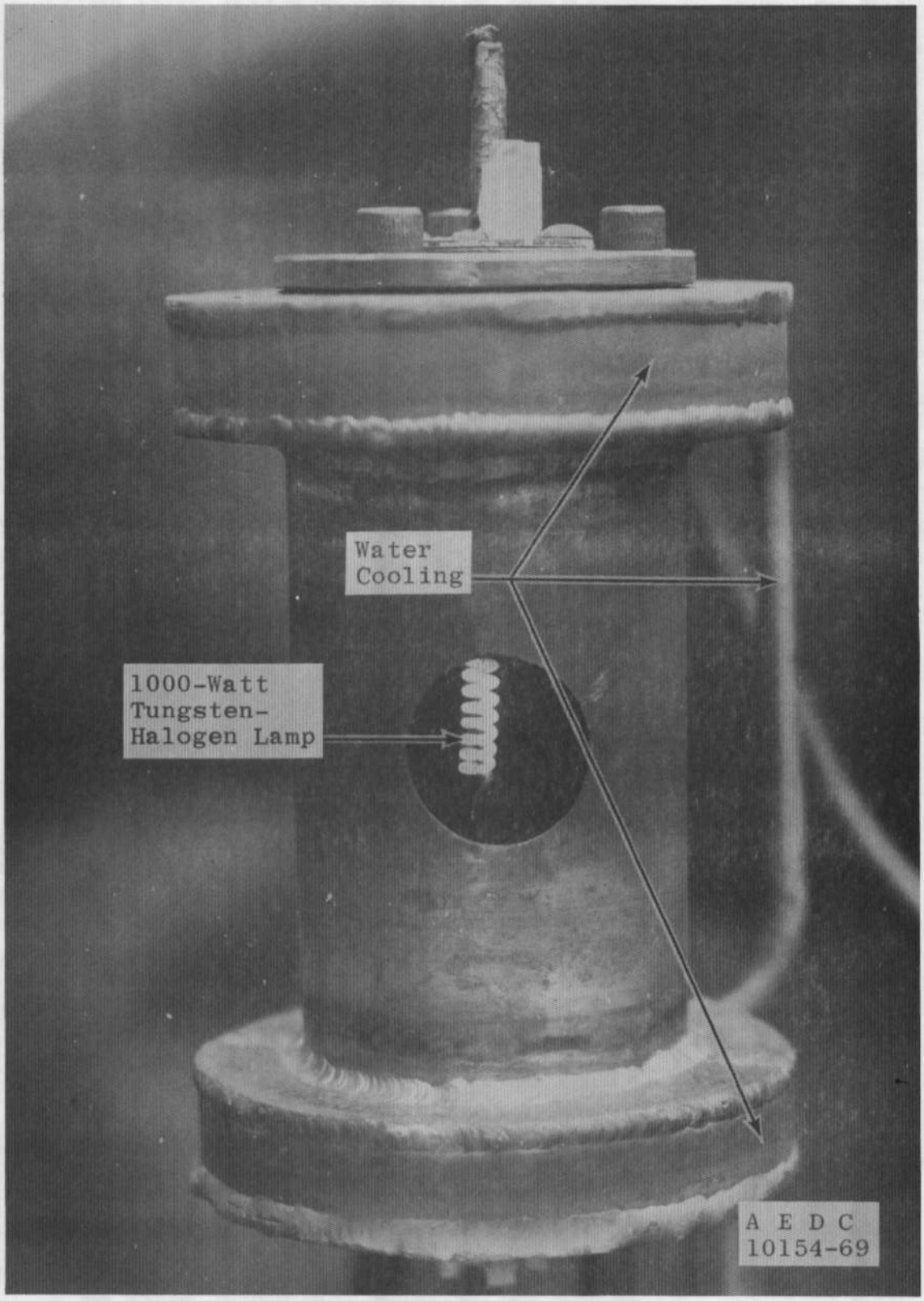

b. Radiation Source
Fig. 3 Concluded

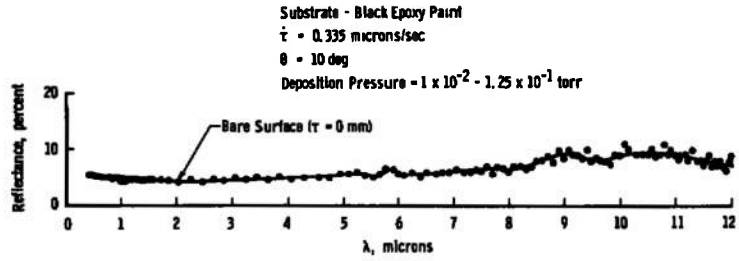

a. $\tau = 0$

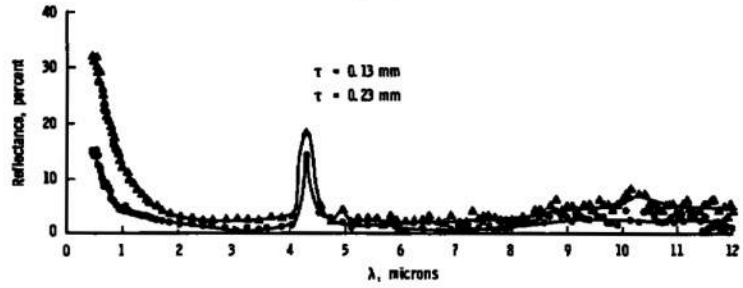

b. $\tau = 0.13$ and 0.23 mm

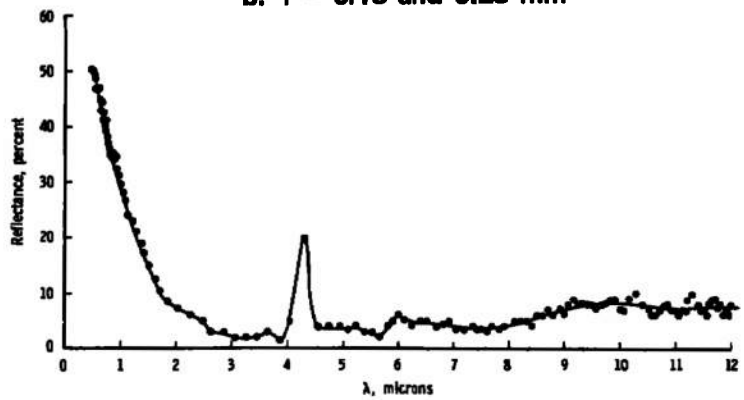

c. $\tau = 0.44$ mm

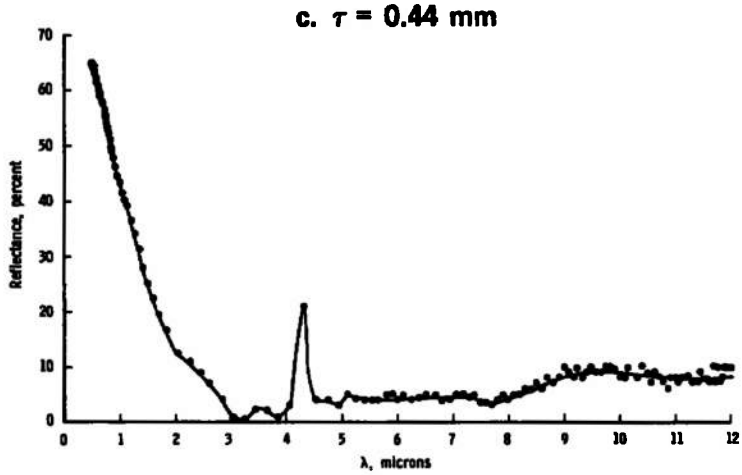

d. $\tau = 0.86$ mm

Fig. 4 Reflectance of CO_2 Cryodeposits Formed on a Black Epoxy Paint Substrate

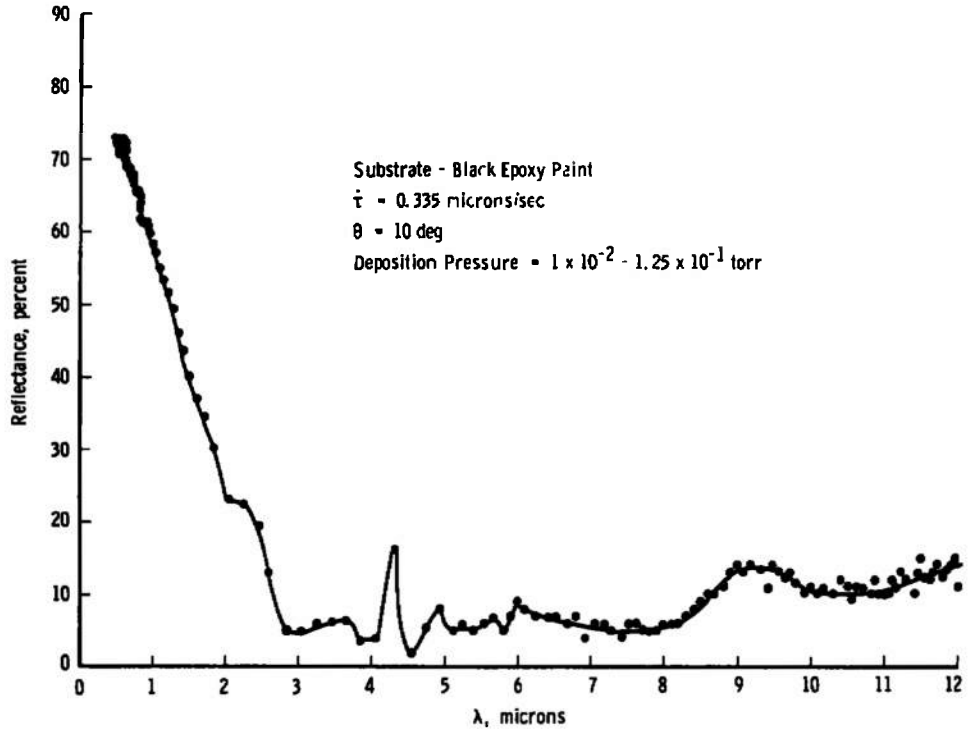

e. τ = 1.70 mm

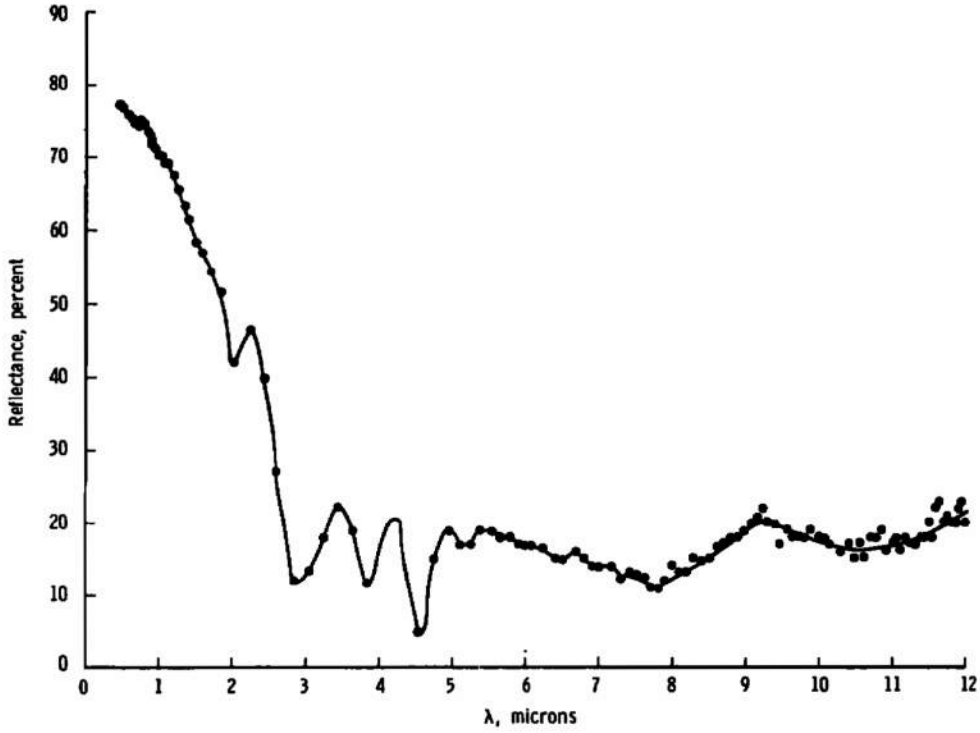

f. τ = 3.38 mm

Fig. 4 Concluded

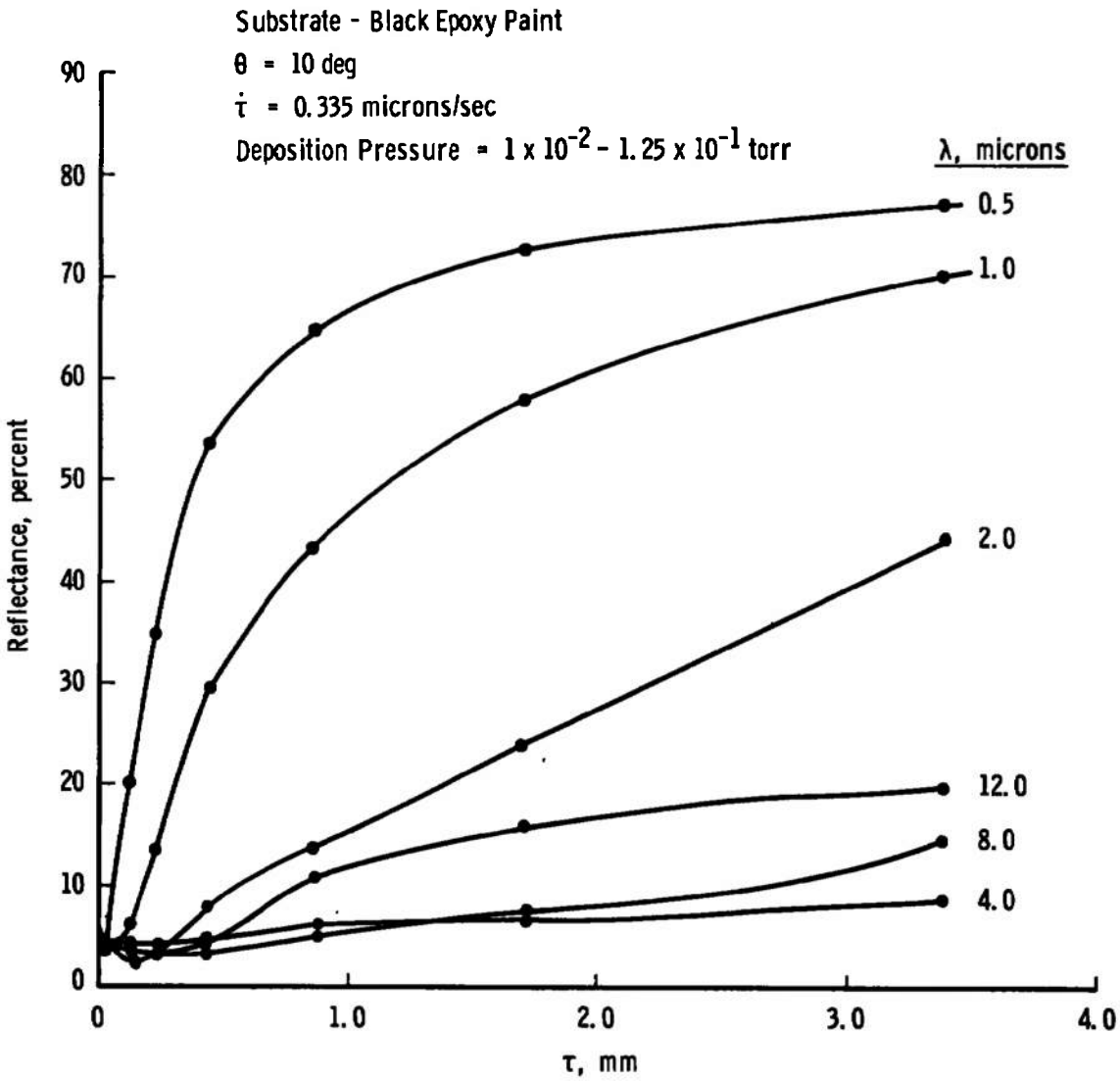

Fig. 5 Reflectance as a Function of CO_2 Deposit Thickness Formed on a Black Epoxy Paint Substrate

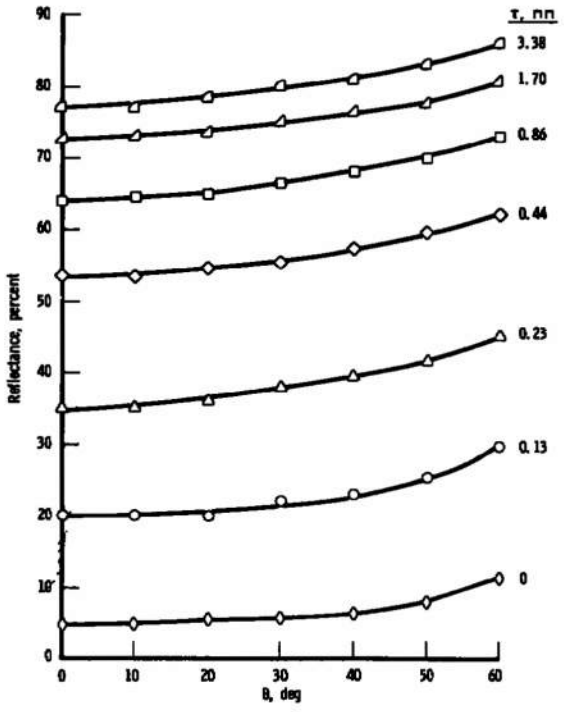

a. λ = 0.5 microns

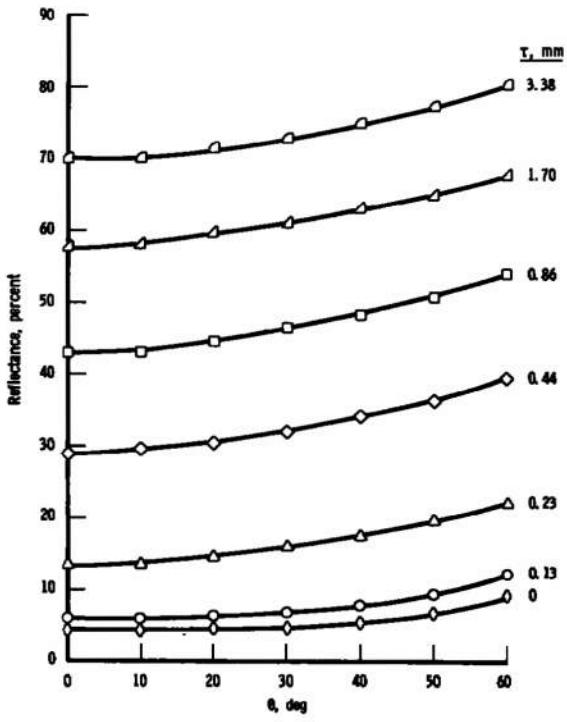

b. λ = 1.0 microns

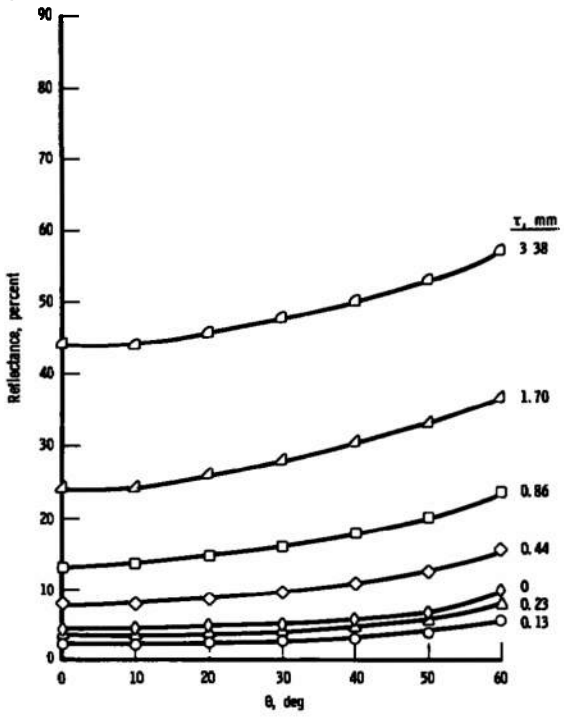

c. λ = 2.0 microns

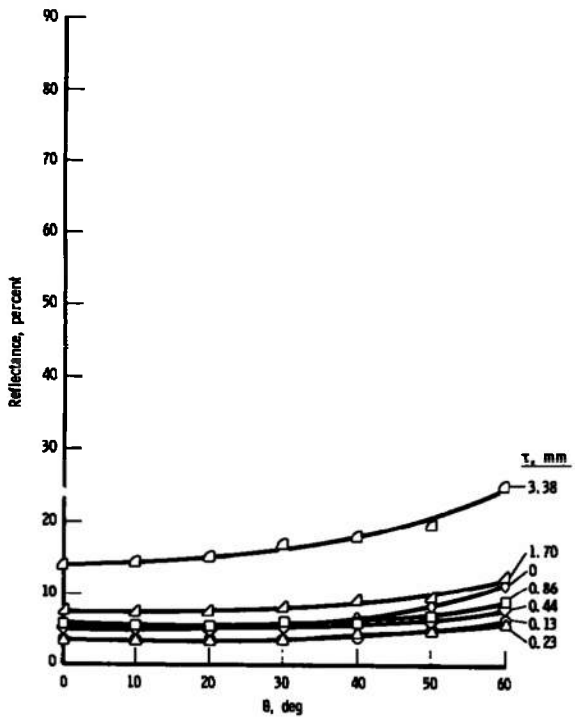

d. λ = 8.0 microns

Fig. 6 Reflectance of CO_2 Deposits Formed on a Black Epoxy Paint Substrate as a Function of View Angle

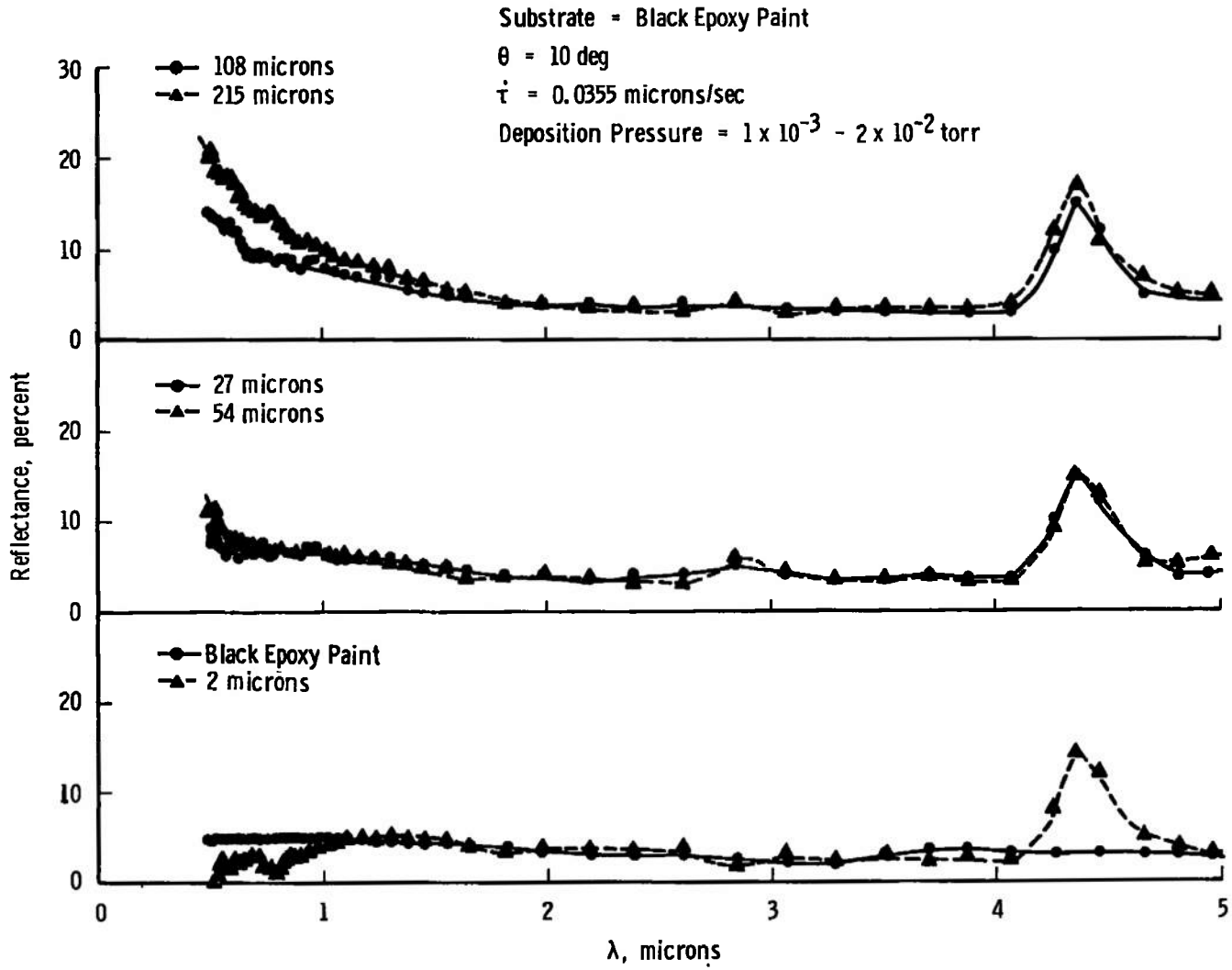

Fig. 7 Reflectance of Relatively Thin CO_2 Cryodeposits Formed on a Black Epoxy Paint Substrate at a Deposition Rate of 0.0355 Microns/sec

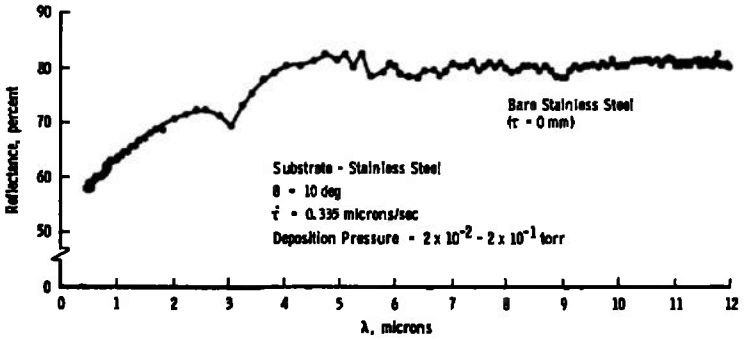

a. $\tau = 0$

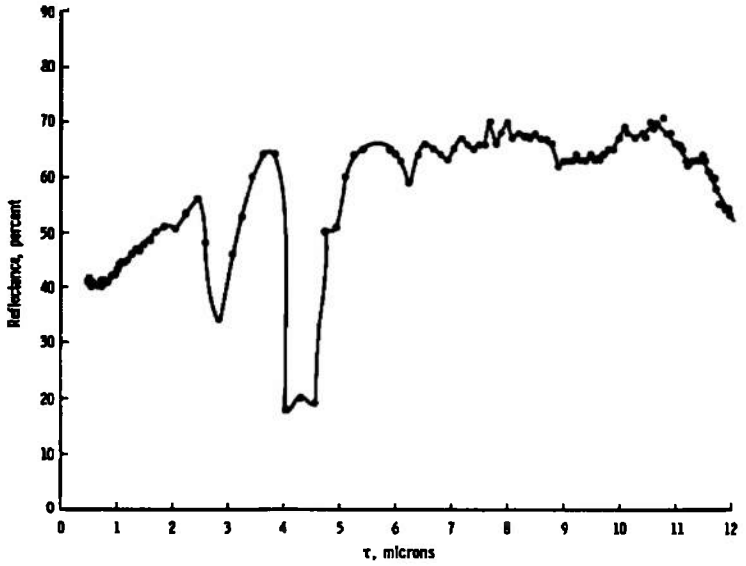

b. $\tau = 0.13$ mm

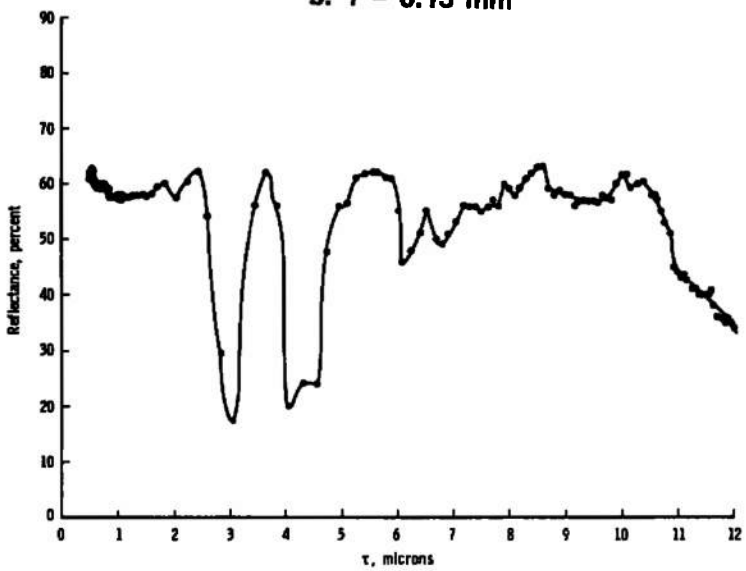

c. $\tau = 0.23$ mm

Fig. 8 Reflectance of CO_2 Cryodeposits Formed on a Stainless Steel Substrate

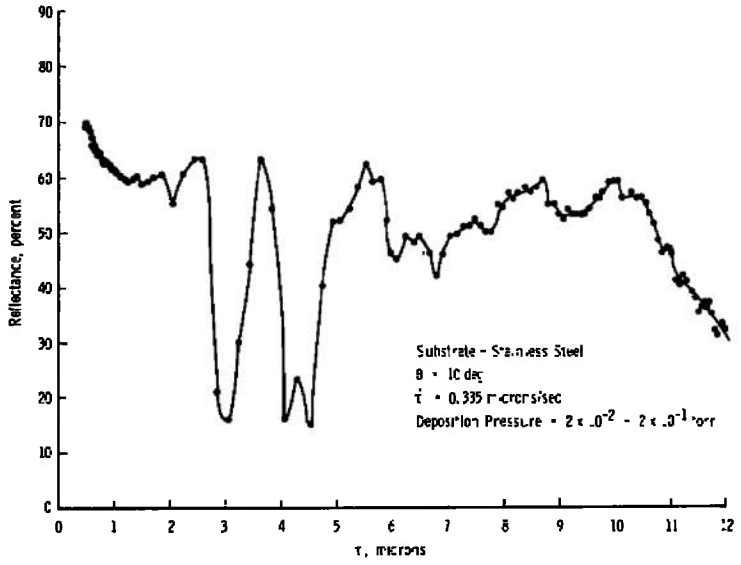

d. τ = 0.44 mm

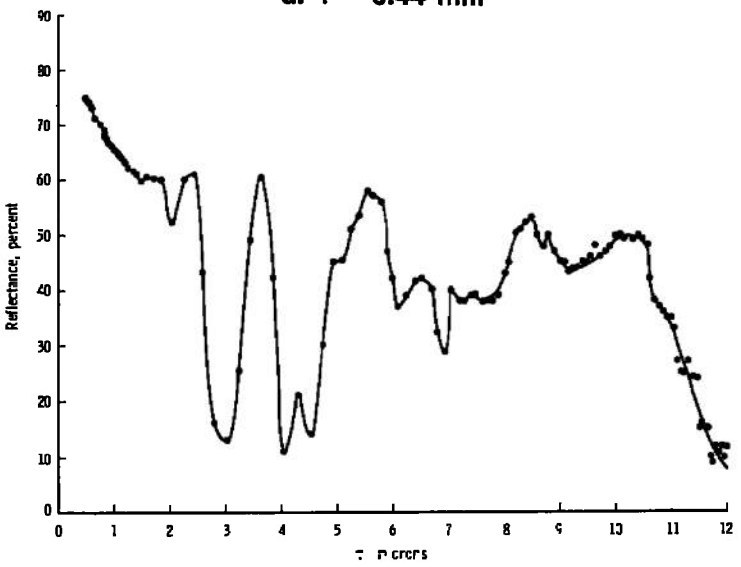

e. τ = 0.86 mm

Fig. 8 Continued

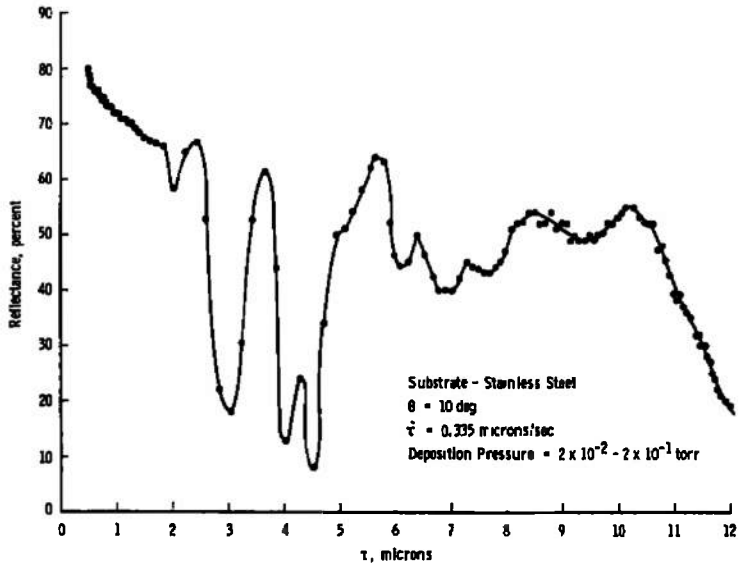

f. τ = 1.70 mm

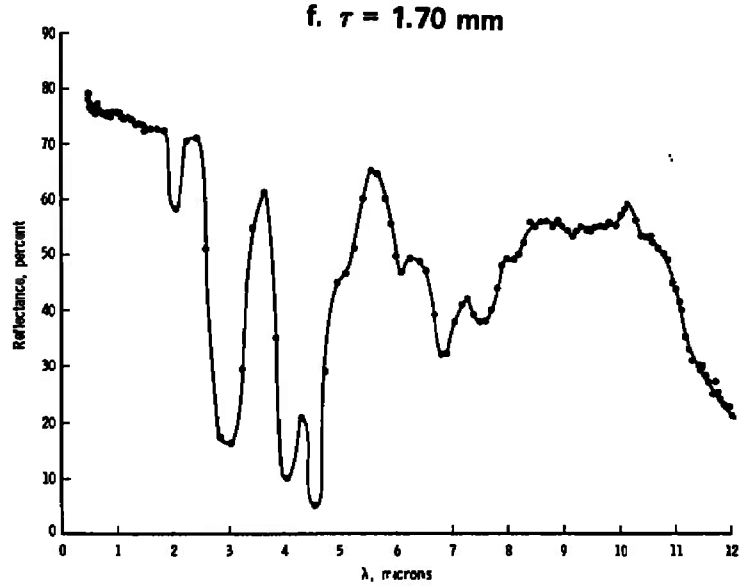

g. τ = 3.38 mm

Fig. 8 Concluded

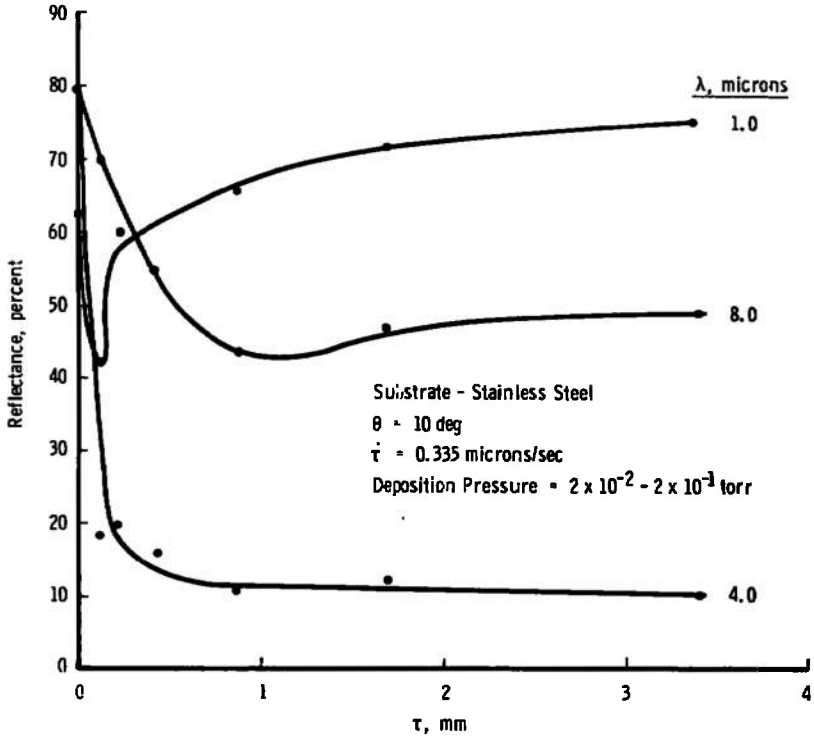

a. λ = 1, 4, and 8 microns

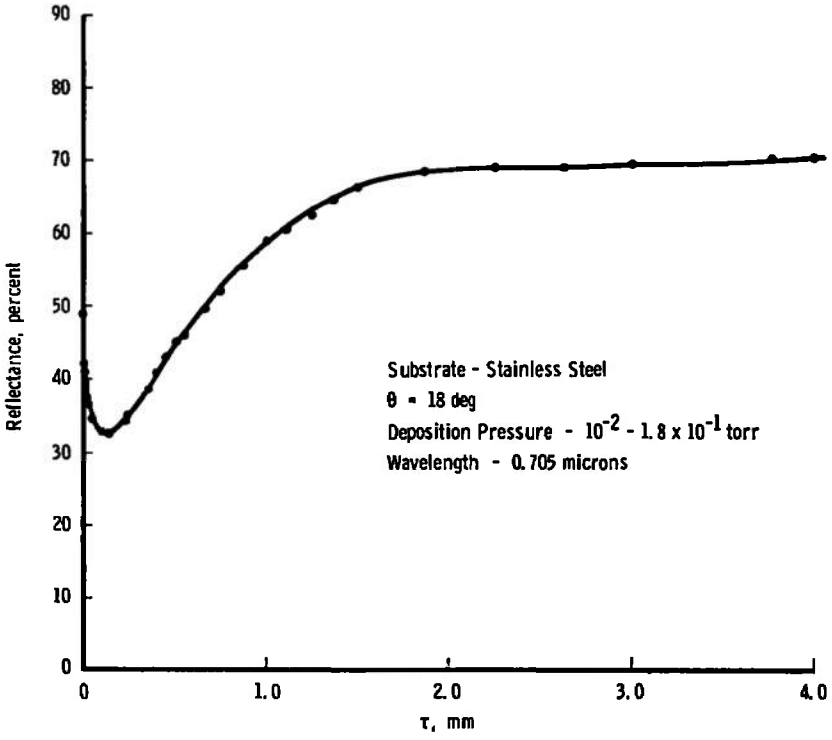

b. λ = 0.7 microns

Fig. 9 Reflectance versus Thickness for CO_2 Deposits Formed on a Stainless Steel Substrate

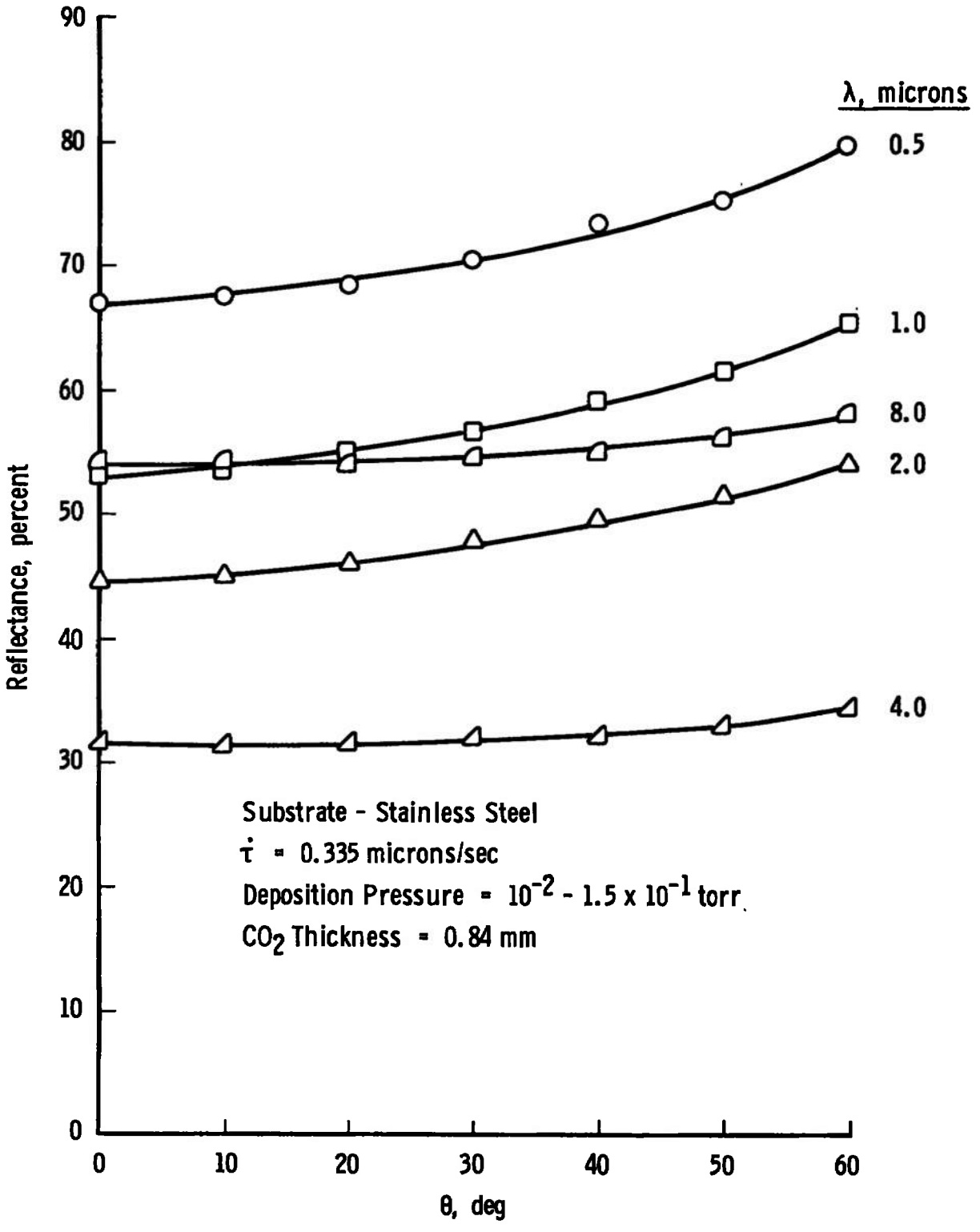

Fig. 10 Reflectance of CO_2 Deposits Formed on a Stainless Steel Substrate as a Function of View Angle

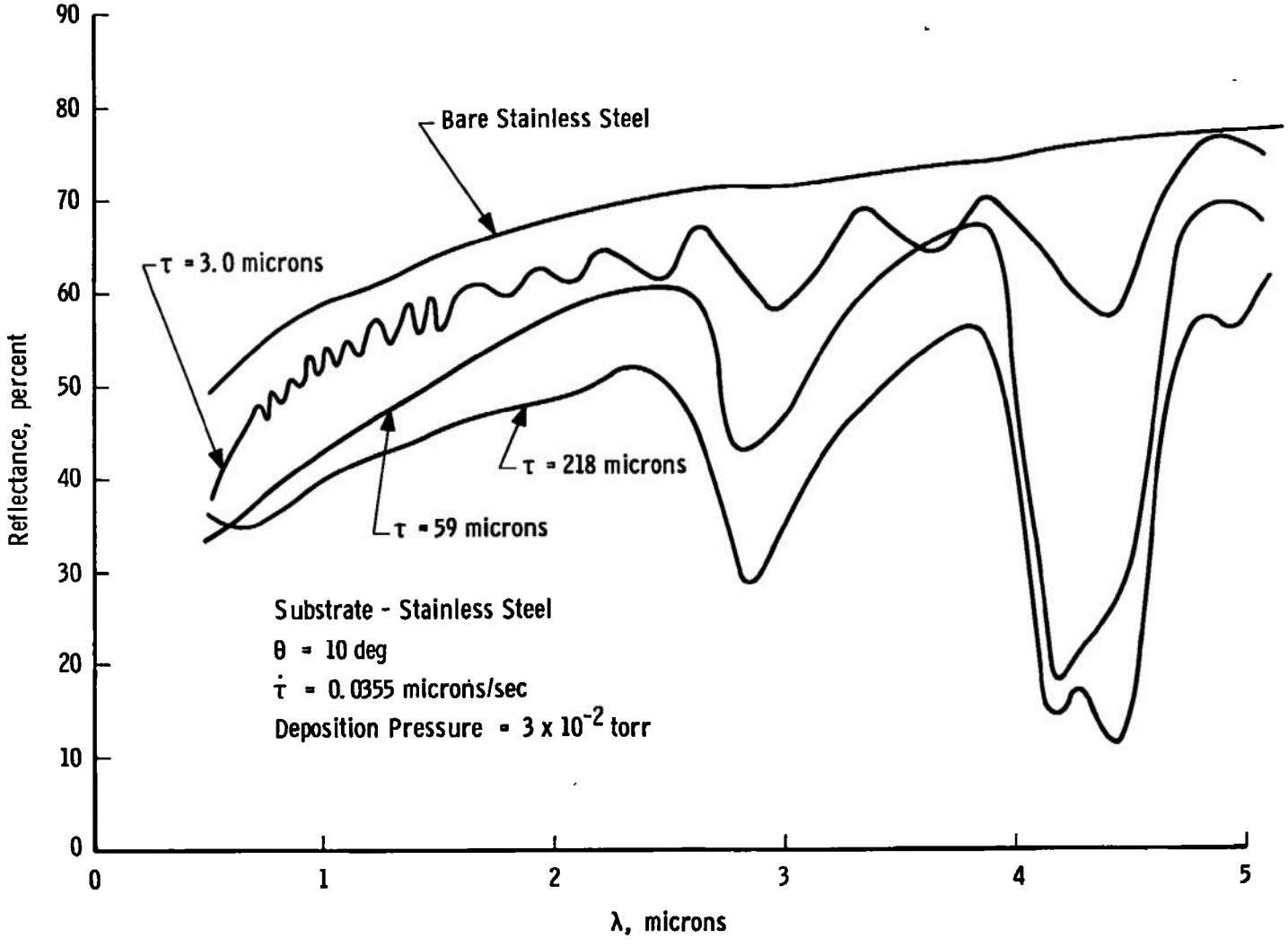

Fig. 11 Reflectance of Relatively Thin CO_2 Deposits Formed on a Stainless Steel Substrate at a Deposition Rate of 0.0355 Microns/sec

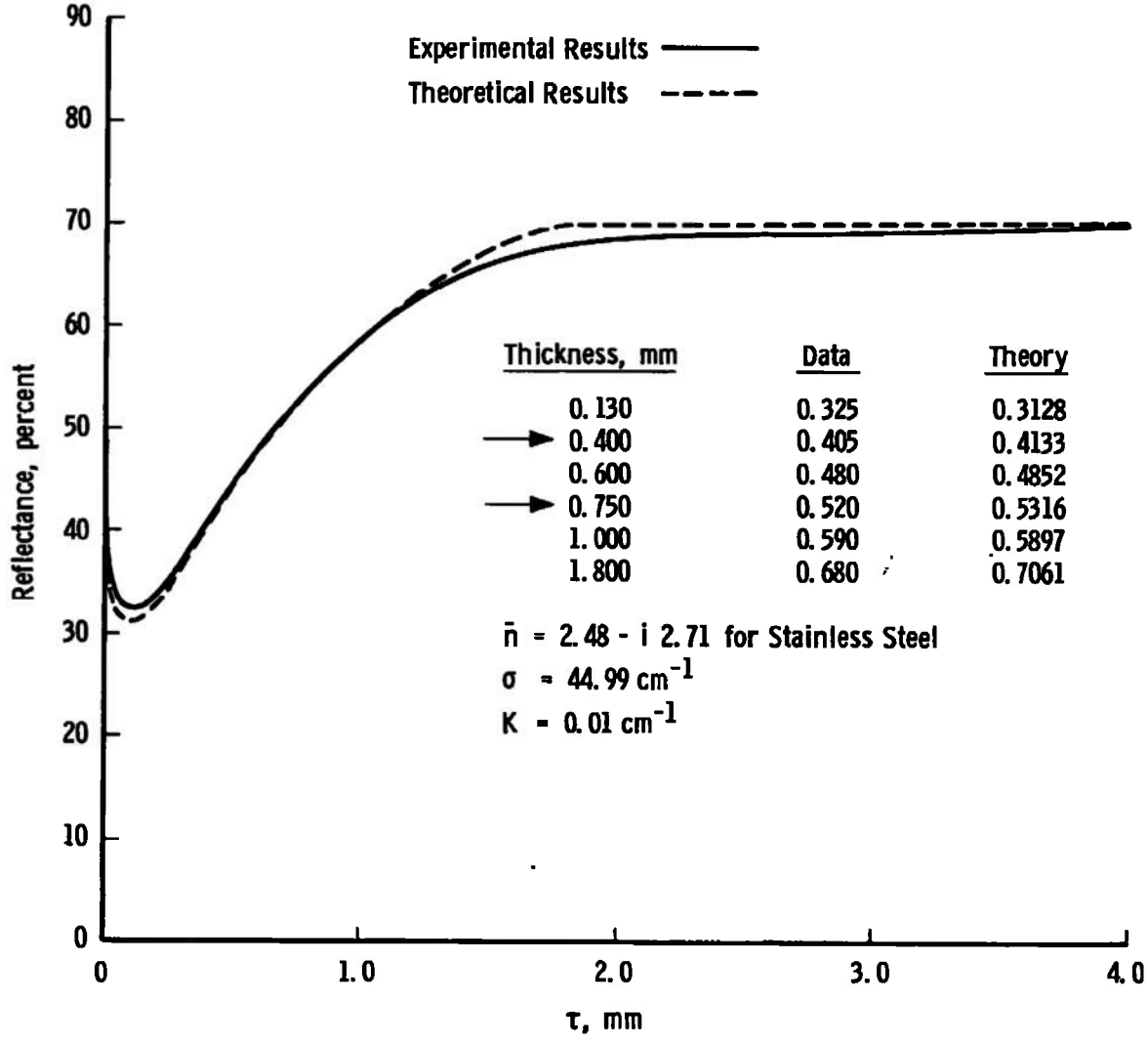

Fig. 12 Comparison of Experimental and Analytical Results for Reflectance versus Thickness of CO_2 Deposits Formed on a Stainless Steel Surface

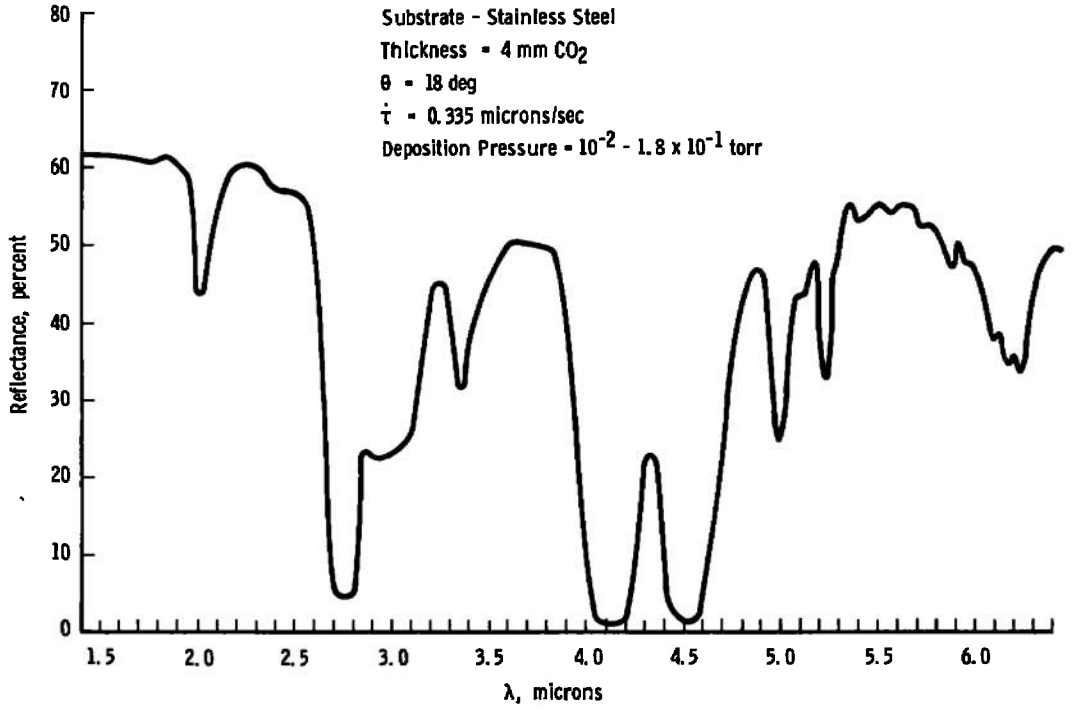

Fig. 13 Reflectance of a 4-mm CO_2 Deposit Formed on Stainless Steel (Data Obtained Using a CaF_2 Prism)

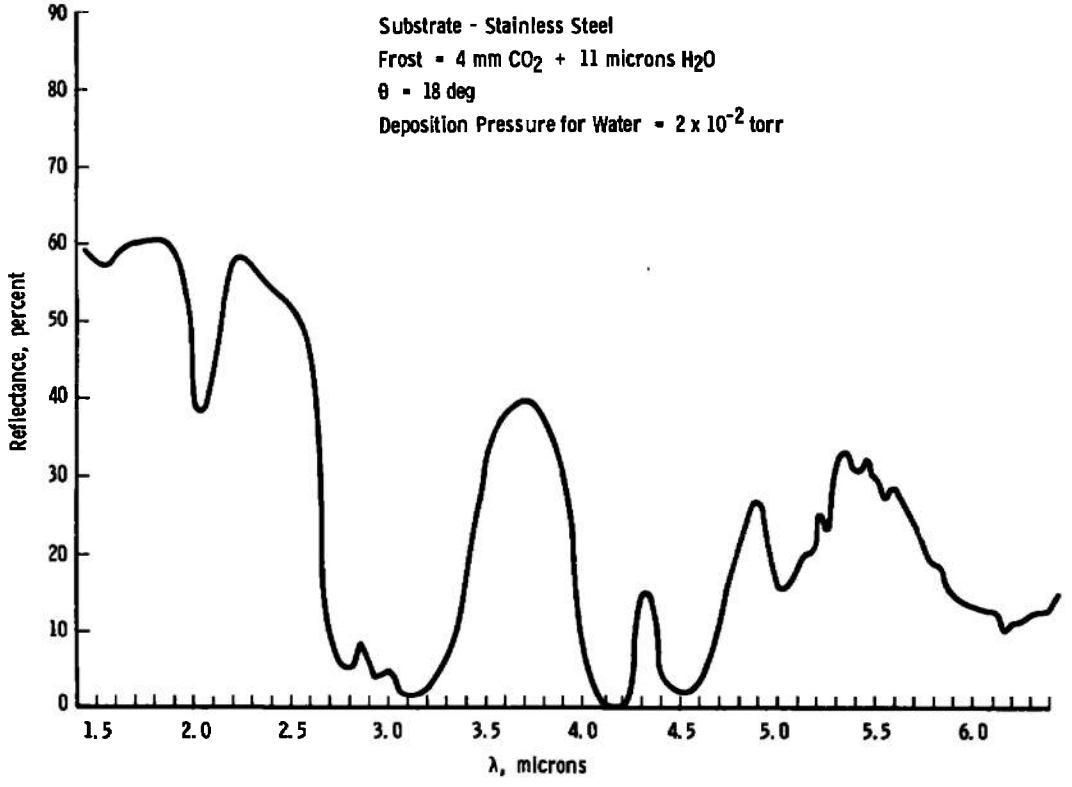

Fig. 14 Reflectance of a 4-mm CO_2 Deposit with a Thin Coating, τ = 11 Microns, of Water Cryodeposit (Data Obtained Using a CaF_2 Prism)

UNCLASSIFIED

Security Classification

DOCUMENT CONTROL DATA - R & D

(Security classification of title, body of abstract and indexing annotation must be entered when the overall report is classified)

1. ORIGINATING ACTIVITY (Corporate author)	2a. REPORT SECURITY CLASSIFICATION
Arnold Engineering Development Center ARO, Inc., Operating Contractor Arnold Air Force Station, Tennessee 37389	UNCLASSIFIED
	2b. GROUP N/A

3. REPORT TITLE

INFRARED REFLECTANCE OF CO_2 CRYODEPOSITS

4. DESCRIPTIVE NOTES (Type of report and inclusive dates)

Final Report July 1968 through September 1969

5. AUTHOR(S) (First name, middle initial, last name)

B. E. Wood, A. M. Smith, B. A. Seiber, et al., ARO, Inc.

6. REPORT DATE	7a. TOTAL NO. OF PAGES	7b. NO. OF REFS
July 1970	39	9

8a. CONTRACT OR GRANT NO.	9a. ORIGINATOR'S REPORT NUMBER(S)
F40600-71-C-0002 b. Program Element 64719F c. d.	AEDC-TR-70-108
	9b. OTHER REPORT NO(S) (Any other numbers that may be assigned this report) N/A

10. DISTRIBUTION STATEMENT

This document has been approved for public release and sale; its distribution is unlimited.

11. SUPPLEMENTARY NOTES	12. SPONSORING MILITARY ACTIVITY
Available in DDC.	Arnold Engineering Development Center, Air Force Systems Command, Arnold AF Station, Tenn. 37389

13 ABSTRACT

In-situ reflectance measurements have been made for carbon dioxide (CO_2) frosts formed on liquid-nitrogen-cooled substrates. The data were obtained spectrally in the wavelength range from 0.5 to 12.0 microns using an infrared integrating sphere. These measurements were made using the hemispherical-angular technique and resulted in the determination of the absolute reflectance. The properties of the CO_2 frosts were studied by forming them on black epoxy paint and polished stainless steel substrates. The CO_2 frosts were found to exhibit an anomalous dispersion reflectance peak at 4.3 microns which was shown to be a very sensitive indication of the presence of solid CO_2. In addition, it was found that CO_2 scatters short wavelength radiation ($\lambda < 1.0$ microns) significantly and is semitransparent for much of the wavelength range between 2.0 and 12.0 microns. The application of these results to other problems associated with cryogenically cooled surfaces is discussed.

DD FORM 1 NOV 65 1473

UNCLASSIFIED

Security Classification

14 KEY WORDS	LINK A		LINK B		LINK C	
	ROLE	WT	ROLE	WT	ROLE	WT
infrared absorption						
Mars (planet)						
cryogenics						
solidified gases						

AFSC
Arnold AFS Tenn